



HAL
open science

Near real-time PM1 chemical composition measurements at a French urban background and coastal site under industrial influence over more than a year: Temporal variability and assessment of sulfur-containing emissions

Shouwen Zhang, Emmanuel Tison, Sébastien Dusanter, Charles Beaugard, Cyril Gengembre, Patrick Augustin, Marc Fourmentin, Hervé Delbarre, Véronique Riffault

► To cite this version:

Shouwen Zhang, Emmanuel Tison, Sébastien Dusanter, Charles Beaugard, Cyril Gengembre, et al.. Near real-time PM1 chemical composition measurements at a French urban background and coastal site under industrial influence over more than a year: Temporal variability and assessment of sulfur-containing emissions. *Atmospheric Environment*, 2021, 244, pp.117960. 10.1016/j.atmosenv.2020.117960 . hal-02975490

HAL Id: hal-02975490

<https://hal.science/hal-02975490>

Submitted on 17 Oct 2022

HAL is a multi-disciplinary open access archive for the deposit and dissemination of scientific research documents, whether they are published or not. The documents may come from teaching and research institutions in France or abroad, or from public or private research centers.

L'archive ouverte pluridisciplinaire **HAL**, est destinée au dépôt et à la diffusion de documents scientifiques de niveau recherche, publiés ou non, émanant des établissements d'enseignement et de recherche français ou étrangers, des laboratoires publics ou privés.



Distributed under a Creative Commons Attribution - NonCommercial 4.0 International License

Near real-time PM₁ chemical composition measurements at a French urban background and coastal site under industrial influence over more than a year: Temporal variability and assessment of sulfur-containing emissions

Shouwen Zhang^{1,2*}, **Emmanuel Tison**¹, **Sébastien Dusanter**¹, **Charles Beaugard**³, **Cyril Gengembre**², **Patrick Augustin**², **Marc Fourmentin**², **Hervé Delbarre**², **Véronique Riffault**^{1‡}

¹ IMT Lille Douai, Univ. Lille, SAGE - Sciences de l'Atmosphère et Génie de l'Environnement, F-59000 Lille, France

² Université du Littoral Côte d'Opale, Laboratoire de Physico-Chimie de l'Atmosphère, F-59140, Dunkerque, France

³ Atmo Hauts de France, F-59000, Lille, France

* now at Atmo Hauts-de-France, F-59000, Lille, France

‡ Correspondence to: Véronique Riffault (veronique.riffault@imt-lille-douai.fr)

1 **Abstract**

2 Near real-time measurements of submicron particulate matter (PM_1) were carried out at an
3 industrial and coastal site in Dunkirk (Northern France) over a 14-month period (July 2013-
4 September 2014). This site is surrounded by various industrial plants (metallurgy,
5 petrochemistry, food processing, power plant, etc.) and is characterized by intense ship traffic
6 (~700-800 per day along the English Channel) in harbour surroundings. The non-refractory
7 (NR) submicron particles (organics, sulfate, nitrate, ammonium and chloride) and black
8 carbon were measured by an Aerosol Chemical Speciation Monitor (ACSM) and an
9 Aethalometer, respectively. Concomitant monitoring of CO_2 , SO_2 , and meteorological
10 parameters was also performed. Both the seasonal (five seasons including two summers) and
11 spatial (four identified sectors of emissions: marine, urban, industrial-urban and industrial)
12 variabilities were investigated.

13 We present a descriptive analysis of the PM_1 composition, whose ambient concentrations
14 ranged from less than $1 \mu g m^{-3}$ up to approximately $100 \mu g m^{-3}$ during a few pollution events.
15 Gaseous SO_2 and particulate SO_4 were systematically observed at high concentrations (up to
16 310 and $48.2 \mu g m^{-3}$, respectively) when industrial plumes reached the monitoring site. The
17 conversion ratio of particulate (S_p) to total (S_{tot}) sulfur is relatively constant at 0.1 when RH
18 ranges from 30-70% but reaches an average value of 0.3 at high RH (90-100%). This reflects
19 an enhancement of SO_2 -to- SO_4 gas-particle conversion processes resulting in an increase of
20 aerosol acidity as shown by a comparison between measured and predicted NH_4
21 concentrations. An impact of the vertical mixing on the SO_2 -to- SO_4 conversion was also
22 observed using vertical turbulence (σ_w) as a descriptive parameter. Indeed, the conversion
23 ratio (S_p/S_{tot}) was found to be reduced under high turbulence conditions due to dilution
24 effects.

25

26 **Keywords:** ACSM, Aethalometer, Submicron particulate matter, Industrial area

27 **1 Introduction**

28 Atmospheric aerosols from both natural and anthropogenic sources have been widely studied
29 during the last decades to assess their influence on climate. Indeed, their optical properties
30 (light scattering and absorption) and their ability to act as cloud condensation nuclei
31 (Flossmann et al. 1985, Ghan and Schwartz 2007) can significantly impact the Earth's
32 radiative balance. In addition, aerosols can strongly impair human health (Pope et al. 2002,
33 Kelly and Fussell 2012, Leclercq et al. 2017) and the wellbeing of ecosystems (Bouwman et
34 al. 2002, Niyogi et al. 2004). Based on their ability to deposit in the respiratory tract, aerosols
35 are classified as PM₁₀, PM_{2.5}, and PM₁, characterized by aerodynamic diameters lower than
36 10, 2.5 and 1 micrometers, respectively. The World Health Organization (WHO) estimates
37 that PM_{2.5} contributes to approximately 0.8 million deaths per year and ranked it as the 13th
38 cause of global mortality (WHO 2002, Cohen et al. 2005, Elder et al. 2009). In the urban
39 environment, PM₁ exhibits a stronger impact on human health than PM_{2.5} since (i) they can
40 penetrate further into the alveolar region, (ii) their chemical composition is dominated by
41 anthropogenic sources and (iii) they lead to a more intense pro-inflammatory response (Pérez
42 et al. 2008, Ramgolam et al. 2009, Kelly and Fussell 2012, Mazzearella et al. 2012).

43 Submicron non-refractory particulate matter (NR-PM₁) can be characterized at a high time
44 resolution using Aerosol Mass Spectrometers (AMS) during short field campaigns over a few
45 weeks. Details about both the chemical composition (organics, nitrate, sulfate, ammonium and
46 chloride) and the size distribution at temporal resolutions of a few minutes have been obtained
47 worldwide (Jayne et al. 2000, DeCarlo et al. 2006, Canagaratna et al. 2007, Zhang et al. 2007,
48 Jimenez et al. 2009). However, despite the unique qualities of an AMS to provide chemical
49 information on PM₁, this type of instruments exhibits several drawbacks for long-term
50 monitoring, such as the need for frequent calibrations and highly skilled operators.

51 More recently, the Aerosol Chemical Speciation Monitor (ACSM) (Aerodyne Research, Inc.)
52 was designed and proposed for long-term monitoring (Ng et al. 2011). In contrast to an AMS,
53 ACSMs do not provide the particle size distribution and exhibit a lower mass resolution,
54 which in turn leads to fewer details about the organic composition. However, ACSM
55 instruments do not require frequent calibrations, are less expensive, and are easier to use
56 during field measurements. It is interesting to note that AMS and ACSM instruments have
57 been already compared several times. A 3-week campaign performed at Queens College (New
58 York, USA) in 2010 showed good correlations (R^2 of 0.81–0.91, slopes of 0.76–1.01)
59 between the two techniques for all measured species (organics, nitrate, sulfate, ammonium
60 and chloride) (Ng et al. 2011). A larger scale intercomparison exercise involving 13 Q-ACSM

61 and one HR-ToF-AMS in Paris (Crenn et al. 2015) showed good agreements between the
62 different instruments with R^2 values higher than 0.9, except for chloride, and slopes ranging
63 from 0.62 to 1.43 depending on the species considered.

64 Industrial activities are important sources of anthropogenic Particulate Matter (PM) (Taiwo et
65 al. 2014, Riffault et al. 2015). However, previous sampling sites where AMS and ACSM
66 instruments have been deployed were usually located in urban, suburban or rural background
67 regions and only a few were impacted by industrial emissions (El Haddad et al. 2013,
68 Budisulistiorini et al. 2015). In Europe, industrial processes represent the third (9.1%) and
69 second (28.6%) primary sources of $PM_{2.5}$ and PM_{10} (EEA 2015), respectively. In France itself,
70 industrial sources accounted for 22% and 29% of $PM_{2.5}$ and PM_{10} in 2012, respectively
71 (CGDD 2014). Of interest for the present study, the Hauts-de-France (HdF) region in France
72 is still heavily industrialized, with industries contributing to 68 and 61% of $PM_{2.5}$ and PM_{10}
73 emissions, respectively, in the Dunkirk conurbation (AtmoHdF 2012).

74 Dunkirk, located in northern France, is impacted by industrial activities such as metallurgy,
75 petrochemistry, food processing, power plant, etc., and is also the first energy platform in
76 HdF. This industrial activity results in massive emissions of gaseous and particulate
77 pollutants, including for the year 2011 Volatile Organic Compounds (VOCs; 1,556 tons),
78 oxides of nitrogen (NO_x , 8,195 tons), sulfur dioxide (SO_2 , 11,752 tons), and particulate matter
79 (10 nm-100 μm ; 3,246 tons) (DREAL 2012).

80 Previous studies focusing on particulate matter in Dunkirk have investigated concentrations in
81 heavy metals (Alleman et al. 2010, Mbengue et al. 2014) and inorganic species (Rimetz-
82 Planchon et al. 2008) in PM_{10} . The organic fraction has also been studied in $PM_{2.5}$ using
83 offline filter methods (Cazier et al. 2011, Crenn et al. 2017, Crenn et al. 2018) and in PM_{10}
84 using an Aerosol Mass Spectrometer (AMS) (Crenn et al. 2017, Crenn et al. 2018, Setyan et
85 al. 2019). PAHs (Polycyclic Aromatic Hydrocarbons) and sulfate in NR- PM_{10} have been found
86 almost exclusively in winter for air masses coming from the industrial zone. However, the
87 filter methods required long sampling times (typically 24-72 hours), precluding any
88 investigation of fast changes in aerosol composition and levels. The two campaigns
89 employing an AMS were only performed for short periods (summer and winter,
90 approximately 1 month each), with only a few wind occurrences from the industrial sector.

91 Volatile Organic Compounds (VOCs), considered as potential precursors of organic aerosols,
92 have also been investigated in Dunkirk (Badol et al. 2008, Badol et al. 2008, Roukos et al.
93 2009). Badol et al. (2008) carried out a measurement campaign of about one year and
94 identified 53 VOCs (Badol et al. 2008). Daily profiles, seasonal variations and pollution roses

95 observed for these compounds indicated strong impacts of traffic, solvent evaporation and
96 industrial emissions on the measured concentrations. In addition, a Chemical Mass Balance
97 (CMB) source-receptor model was applied to estimate the contributions of various emission
98 sources, including 6 urban profiles and 7 industrial profiles (Badol et al. 2008). Roukos et al.
99 (2009) carried out two measurement campaigns in summer and winter 2007 using passive
100 sampling on adsorbent cartridges (Roukos et al. 2009). This study showed that pollution
101 transported over long distances has a significant impact on VOC concentrations in the
102 Dunkirk area during specific weather conditions. Xiang et al. (Xiang et al. 2012) reported a
103 source apportionment study coupling a Positive Matrix Factorization (PMF) analysis and
104 micro-meteorology observations. This study highlighted that an increase of the turbulence
105 could lead to a lower contribution of ground level sources and an enhanced contribution of
106 elevated sources (such as plumes from chimneys).

107 The present study provides the first near real-time and long-term (> 1 year) monitoring of
108 submicron aerosols at an urban background and coastal site strongly impacted by industrial
109 activities (within a few km). This work aims at better understanding PM₁ temporal variability
110 in terms of mass concentration and chemical composition, and their transformation in this
111 complex environment. Organic PM₁ sources will be further investigated using PMF in a
112 forthcoming paper. The database of PM₁ measurements is analyzed by seasons and wind
113 sectors to investigate the origin of local emissions. Particular attention was paid to the impact
114 of industrial sulfur emissions on the formation of sulfate particles.

115

116 **2 Experimental section**

117 **2.1 Campaign description**

118 The measurement site was located on the eastern side of the Dunkirk harbour (Port-Est, PE:
119 51°3.12' N; 2°21.24' E; 1 m). This site is surrounded, within a few kilometers, by an
120 intensive industrial zone at W-SW and by a residential zone at S-SE as shown in Figure 1.
121 This geographical location allows classifying the origin of local air masses according to four
122 wind sectors: marine (M; 271° -70°), urban (U; 71° - 140°), industrial-urban (IU; 141° -
123 225°), and industrial (I; 226° - 270°). This site can sometimes be under the influence of
124 remote sources from France, Belgium, England, and Germany within a few tens to hundreds
125 of kilometers.

126 The field campaign was conducted over 14 months from July 15, 2013 to September 10,
127 2014. An ACSM and an Aethalometer (described below) were installed at the PE site,
128 alongside an SO₂ analyzer (AF21M, Environnement SA) managed by the Atmo HdF regional

129 air quality monitoring network and a CO₂ analyzer (VS-3000, HORIBA). The SO₂ analyzer
130 was operated continuously at a time resolution of 15 min and was calibrated once a month
131 using a SO₂ gas standard at 200 ppb (Air Liquide). The CO₂ analyzer was calibrated 3 times
132 during the campaign, using a CO₂ gas standard at 997 ppm (purity > 99.9%, Praxair). An
133 ultrasonic anemometer (uSonic-3 Scientific, METEK) was deployed at a nearby site
134 approximately 1 km away (Figure 1) for measuring horizontal and vertical wind speeds and
135 direction, as well as temperature and turbulence parameters. Standard meteorological
136 parameters such as temperature, relative humidity, precipitation, pressure, and solar radiation
137 were also recorded on the rooftop of a research building of the Université du Littoral Côte
138 d'Opale (51°2.14'N; 2°22.05'E), located at 2 km. From June 23, 2014 to September 10, 2014,
139 an ambient particulate monitor (TEOM-FDMS 1405-F, Thermo Fischer Scientific) was
140 additionally deployed to measure the total PM₁ mass concentration. Section A of the
141 Supplementary Information reports the number of valid data (Table S1) as well as the
142 temporal data coverage (Figure S1) for each instrument. Measurements were averaged over
143 the ACSM time stamp using Coordinated Universal Time (UTC).

144

145 **2.2 PM₁ chemical composition**

146 **2.2.1 Aerosol Chemical Speciation Monitor (ACSM)**

147 The ACSM (Aerodyne Research Inc.) provides measurements of particulate organics, nitrate,
148 sulfate, ammonium and chloride in the non-refractory submicron particles (Ng et al. 2011).
149 The aerodynamic lens inside the ACSM inlet sampled PM₁ at a flow rate of approximately 80
150 cm³ min⁻¹, controlled by a 100 μm diameter critical aperture. Non-refractory components
151 were vaporized at 600°C after impaction on an inverted-cone surface and then ionized by
152 electron impact at 70 eV. A RGA (residual gas analyzer) quadrupole mass spectrometer was
153 used to acquire mass spectra at a mass resolution of one unit and up to 148 amu. During
154 acquisition, the ACSM was operated with a three-way automatic valve to switch between the
155 filter mode (particle-free air) and the sample mode (ambient air). The difference between
156 these two modes is considered as the signal generated by ambient aerosols. The scan speed
157 was set to 200 ms amu⁻¹. 28 scans were acquired for both the filter and the sample modes,
158 resulting in a time resolution of approximately 30 min. The instrument was installed in an air-
159 conditioned room (20°C) for continuous monitoring.

160 Ambient aerosols were sampled through a PM_{2.5} cyclone (URG-2000-30EQ) at a flow rate of
161 3 L min⁻¹ and a stainless-steel tube whose length and inner diameter were 2.1 m and 1.27 cm,
162 respectively (residence time in the sampling tube was approximately 5 seconds). The particle

163 size-dependent loss due to the sampling setup was calculated using the Particle Loss
 164 Calculator (PLC) (von der Weiden et al. 2009), and was found to be negligible (< 1%).
 165 Sampled aerosols were dried using a Nafion dryer (PD-200T-12 MPS, Perma Pure) reaching a
 166 relative humidity (RH) always lower than 30%, which is important to minimize the effect of
 167 RH on the collection efficiency (CE) as discussed later in this section.
 168 The mass spectra acquired by ACSM were analyzed using a fragmentation table (Allan et al.
 169 2004, Canagaratna et al. 2007) to extract distinct chemical species or group of species. The
 170 mass concentration of a species s (C_s) is derived from the measured ion current $IC_{s,i}$ (amperes)
 171 using Equation (1):

$$172 \quad C_s = \frac{CE_s}{T_{m/z}} \times \frac{10^{12}}{RIE_s} \times \frac{Q_{cal} \times G_{cal}}{RF_{NO_3}} \times \frac{1}{Q \times G} \sum_{alli} IC_{s,i} \quad (1)$$

173 where $\sum IC_{s,i}$ is the sum of the ensemble mass spectrum fragment i contributing to species s ;
 174 CE_s is the collection efficiency of a species s ; $T_{m/z}$ the ion transmission efficiency; RF_{NO_3}
 175 (ions/molecule) the response factor for NO_3 ; and RIE_s the relative ionization efficiency of a
 176 species s compared to NO_3 ; Q_{cal} and G_{cal} are the volumetric sample flow rate ($cm^3 s^{-1}$) and
 177 multiplier gain ($\sim 20,000$) measured during calibrations of RF_{NO_3} , respectively. In general,
 178 values of Q and G observed during ambient measurements are similar to the values measured
 179 during calibration experiments (Q_{cal} and G_{cal}) and these parameters cancel out in Eq. (1).

180 The instrument calibration protocols and signal optimization are based on existing procedures
 181 (Ng et al. 2011) and are presented in more details in the Supplementary Information (section
 182 B). The NO_3 response factor (RF_{NO_3}) and the relative ionization efficiency (RIE_s) were
 183 calibrated at the beginning and periodically during the campaign (once per month). Average
 184 values of RF_{NO_3} (3.81×10^{-11}) and RIE_s (NH_4 : 5.67; SO_4 : 0.55; Cl : 2.26) were used for the
 185 whole campaign. For organics, the default value of $RIE(1.4)$ was used (Jimenez et al. 2003).
 186 The RF_{NO_3} and RIE_{NH_4} values observed in the present study are close to the average value of
 187 13 Q-ACSM used during the intercomparison exercise described by Crenn et al. (Crenn et al.
 188 2015), i.e. 3.55×10^{-11} and 6.31, respectively. Most previous studies used the default values
 189 of 1.2 for SO_4 (Ng et al. 2011) and 1.3 for Cl (Alfarra et al. 2004) but $RIE(SO_4)$ has been
 190 found to vary from one instrument to another (Ng et al. 2011).

191 The CE of a species s is mainly influenced by particle humidity (for $RH > 80\%$), acidity, and
 192 the mass fraction of ammonium nitrate (Matthew et al. 2008). Humidity effects are ignored in
 193 the present study because particles were dried at RH below 30%. However, both particle
 194 acidity and the fraction of ammonium nitrate were taken into consideration for the calculation

195 of CE, using the method described by Middlebrook et al. (Middlebrook et al. 2011) and
196 described in the Supplementary Information (section C) where the CE time series can be
197 found (Figure S1). More than 57% of the CE values were at 0.45 and the rest ranged from
198 0.45-0.9 during the campaign.

199 As the ACSM is equipped with a quadrupole mass spectrometer, the m/z -dependent ion
200 transmission efficiency ($T_{m/z}$) is assessed using an internal naphthalene standard whose parent
201 ion is detected at m/z 128 and several fragments are detected at lower m/z . Finally, a
202 reference period was chosen when the signal of air beam ($m/z = 28$, corresponding to N_2^+) is
203 stable and as close as possible to 10^{-7} A. This normalization takes into account the variation of
204 air beam over time, as well as the changes in the detector sensitivity and flow rate.

205 ACSM data were acquired using ACSM_DAQ_v1438 at a time resolution of 30 min and
206 processed using ACSM_Local_v1535 (ARI) with Igor Pro 6.36 (WaveMetrics, Inc., Oregon
207 USA). A total of 15,231 valid observations was recorded, split as follows between the four
208 wind sectors: M – 5,527 (36%), U – 1,257 (8%), IU – 6,590 (43%) and I – 1,857 (12%).

209

210 **2.2.2 Aethalometer**

211 Black carbon was measured with a two-wavelength aethalometer (AE42, Magee Scientific
212 Inc.) at 880 nm. The aethalometer sampled ambient air at a flow rate of 5 liters per minute
213 through a PM_{10} sampling head (SCC-1.197, BGI). Samples were collected at a time resolution
214 of 5 min on a moving tape made of quartz fibers. The tape does not move forward until the
215 spot reaches a certain density (set at 60% in this study). The principle of the aethalometer is to
216 measure the optical attenuation of the collected aerosols and the BC concentration is
217 calculated from the attenuation variation at a wavelength of 880 nm:

$$218 \quad BC_{raw} = \frac{A \times \Delta ATN}{\sigma_{ATN} \times Q \times \Delta t} \quad (2)$$

219 where A is the surface of the sampling area on the filter (1.67 cm^2), Q the volumetric flow rate
220 and ΔATN the variation of the attenuation during the time interval Δt . $\sigma_{ATN} (\text{m}^2 \text{ g}^{-1})$ is the
221 specific attenuation coefficient for BC.

222 However, according to the literature (Virkkula et al. 2007, Park et al. 2010), the relationship
223 between the change in attenuation and BC concentration is not always linear. BC
224 concentrations have been corrected using a procedure proposed by Weingartner et al.
225 (Weingartner et al. 2003) as shown in Eq. (3):

$$BC_{corr} = BC_{raw} \times \frac{1}{C_{ref} \times \left(\frac{1}{m(1 - \omega_0) + 1} - 1 \right) \times \frac{\ln(ATN) - \ln(10\%)}{\ln(50\%) - \ln(10\%)} + 1} \quad (3)$$

where BC_{raw} is the concentration measured by the aethalometer from Eq. (6). C_{ref} and m values of 2.14 and 0.87, respectively, were used in the present study (Petzold et al. 1997, Weingartner et al. 2003). ω_0 , the single scattering albedo (SSA) of the sampled aerosols, was taken from AERONET (AERosol RObotic NETwork, <http://aeronet.gsfc.nasa.gov>) measurements in Dunkirk (N 51°2.1', E 02°22.07') and an average value of 0.9 was used.

2.2.3 Wind and trajectory analyses

The wind and trajectory analyses combine the observed concentrations with wind and air mass conditions, in order to understand the origin of some pollutants, as described in more details in (Boichu et al. 2019) and (Roig Rodelas et al. 2019). Briefly, these analyses were performed using the Zefir tool v.3.70 (Petit et al. 2017). We used (i) the non-parametric wind regression (NWR) model to study the regional vs. local origin of a given pollutant based on local wind speed and direction provided by the ultrasonic anemometer; and (ii) the Concentration-Weighted Trajectory (CWT) method to determine the regions of emissions for transported ammonium and nitrate and/or their precursors, using backtrajectories calculated with HYSPLIT 4 and meteorological data from the Global Data Assimilation System (GDAS) at 1°×1° spatial resolution (Stein et al. 2016). 3-day backward trajectories arriving at 500 m above ground level were calculated every 6 hours over the whole campaign.

3 Results and discussion

3.1 Meteorology

Time series of meteorological parameters are displayed in Figure 2 and their seasonal variability is reported in Table 1. The maximum solar radiation varied roughly from 300 (winter) to 800 $W m^{-2}$ (summer). The seasonal ratio of maximum to mean radiation indicates the impact of cloud coverage. Cloud coverage is on average similar in spring-summer and autumn-winter periods, but the ratio increases by about 50% in autumn and wintertime. Over the whole campaign, pressure and temperature time series are also displayed, with average values of 1013 hPa and 14°C, varying from 978 to 1037 hPa and from 1.4 to 32.2 °C, respectively. The average wind speed was 4.9 $m s^{-1}$, with higher values during fall (5.3 $m s^{-1}$) and winter (5.9 $m s^{-1}$), and lower values during spring (4.7 $m s^{-1}$) and summer

257 (4.2 m s⁻¹). Seasonal mean and maximum pressures indicate clearly an increase of the
 258 frequency of low pressure systems in autumn and winter, corresponding to south-
 259 southwesterly winds from the North Atlantic Ocean.

260 The winter season was mild in 2013-2014, with no frost, but high wind speed events
 261 (>14 m s⁻¹) were observed during 12 days from October to February, including 5 remarkable
 262 storms (Christian, Godehard, Xaver, Dirk and Qumara). The summer was also mild with
 263 moderate temperatures (20-25°C) due to the proximity of the North Sea, and the development
 264 of 18 sea-breeze events. During low wind speed periods, 14 fog events occurred. Rain (> 1
 265 mm/hour) was observed on 51 days, enhancing wet deposition mechanisms of particles.

266 Figure S3 (section D of the SI) shows the seasonal variation of the distribution (normalized to
 267 100%) of sectorial winds according to previously defined ranges of wind directions. The
 268 marine sector exhibited the strongest seasonal variation, with a contribution to the wind
 269 distribution during summers 2013 and 2014 higher than 50% but reduced to ~20% during
 270 winter. The urban sector exhibited a small contribution of ~10% during the whole campaign.
 271 However, even with such a small contribution, air masses originating from this sector can
 272 bring high PM concentrations to the measurement site (see next section). The industrial sector
 273 also exhibited a constant contribution of approximately 10%, independent of the season. The
 274 industrial-urban sector exhibited a larger contribution ranging from 30 to 70% all along the
 275 campaign, especially in winter when southern winds were observed. It is important to note
 276 that the seasonal variability of the wind distribution will be one of the main parameters
 277 driving PM₁ mass and composition variations.

278

279 Table 1. Mean, maximum and minimum values of the main parameters and chemical species
 280 for each season during the entire campaign

		Summer 2013	Autumn 2013	Winter 2013-2014	Spring 2014	Summer 2014
Wind speed (m s ⁻¹)	mean±σ	4.2 ± 2.0	5.3 ± 2.5	5.9 ± 2.5	4.7 ± 2.3	4.2 ± 2.0
	max	12.8	19.1	17.6	12.6	13.7
Radiation* (W m ⁻²)	mean;	296;	132;	149;	306;	291;
	max	968	629	706	982	912
Pressure (hPa)	mean±σ	1018 ± 7	1016 ± 11	1006 ± 12	1015 ± 8	1013 ± 5
	min-max	993 - 1032	980 - 1037	978 - 1032	999 - 1036	995 - 1023
RH (%)	mean±σ	79 ± 11	83 ± 7	83 ± 8	78 ± 11	79 ± 11
	min-max	36 - 96	55 - 98	34 - 100	35 - 97	29 - 96
T (°C)	mean±σ	18.4 ± 2.5	11.8 ± 3.8	9.8 ± 2.4	13.7 ± 3.1	18.4 ± 2.2
	min-max	11.3 - 32.2	1.4 - 21.2	2.6 - 19.2	4.5 - 25.1	11.9 - 32.1
Precip. (mm/hour)	mean±σ	0.01 ± 0.14	0.03 ± 0.15	0.03 ± 0.13	0.01 ± 0.11	0.02 ± 0.27
	max	5	3.4	2.6	4.8	16
SO₂	mean±σ	11 ± 26	8 ± 19	11 ± 22	12 ± 20	10 ± 20

($\mu\text{g m}^{-3}$)	max	310	218	206	206	220
CO ₂	mean $\pm\sigma$	430 \pm 15	428 \pm 16	414 \pm 11	416 \pm 14	415 \pm 12
(ppm)	min-max	391 - 557	364 - 555	367 - 548	370 - 537	388 - 549
BC**	mean $\pm\sigma$	0.7 \pm 0.8	/	0.8 \pm 0.8	0.6 \pm 0.9	0.5 \pm 0.6
($\mu\text{g m}^{-3}$)	max	15.3	/	27.7	28.3	21.7
Org	mean $\pm\sigma$	2.0 \pm 1.8	3.8 \pm 5.1	3.3 \pm 3.2	3.1 \pm 3.0	2.4 \pm 2.1
($\mu\text{g m}^{-3}$)	max	11.8	51.9	70.0	25.2	45.8
SO ₄	mean $\pm\sigma$	2.9 \pm 3.1	2.2 \pm 2.8	1.8 \pm 3.6	2.5 \pm 2.8	2.5 \pm 2.5
($\mu\text{g m}^{-3}$)	max	28.4	23.9	48.2	21.7	31.6
NO ₃	mean $\pm\sigma$	1.3 \pm 2.4	2.7 \pm 4.0	2.5 \pm 3.7	4.1 \pm 4.7	1.6 \pm 2.6
($\mu\text{g m}^{-3}$)	max	15.0	23.0	27.3	21.5	16.2
NH ₄	mean $\pm\sigma$	1.1 \pm 1.1	1.4 \pm 1.7	1.2 \pm 1.7	1.9 \pm 1.6	1.1 \pm 1.1
($\mu\text{g m}^{-3}$)	max	6.1	10.0	21.4	8.0	8.0
Cl	mean $\pm\sigma$	0.03 \pm 0.07	0.09 \pm 0.16	0.06 \pm 0.10	0.06 \pm 0.12	0.02 \pm 0.04
($\mu\text{g m}^{-3}$)	max	1.5	3.2	2.3	2.0	0.7

281 * Radiation represents daytime values computed using only data after sunrise and before sunset.

282 ** BC values are not available in autumn.

283

284 3.2 PM₁ mass concentration and chemical speciation

285 To check the aerosol measurements quality, the total mass concentration of PM₁ measured by
286 the ACSM (NR-PM₁) and the aethalometer (BC) was compared to TEOM-FDMS
287 measurements from June 23 to September 10, 2014 (Figure 3). Figure 3 displays time series
288 of PM₁ from both (i) the ACSM and aethalometer and (ii) the TEOM-FDMS. This figure
289 shows that PM₁ concentrations ranged from less than 1 $\mu\text{g m}^{-3}$ to approximately 50 $\mu\text{g m}^{-3}$
290 during the 2.5 months of the comparison period, with both traces showing similar temporal
291 variations. A scatter plot of the ACSM + aethalometer and TEOM-FDMS measurements is
292 shown in Figure 3b. This figure also displays 24-hour averaged values for both measurements,
293 which indicate an excellent agreement (slope: 0.94; $r^2 = 0.94$), suggesting that (i) most of the
294 PM₁ mass ($7.9 \pm 7.1 \mu\text{g m}^{-3}$ measured by the TEOM-FDMS) is captured by the combination
295 of ACSM and aethalometer ($8.1 \pm 6.3 \mu\text{g m}^{-3}$); (ii) the RF/RIE calibrations and the CE
296 correction applied for the ACSM data analysis are correct within measurement uncertainties.
297 Time series of Cl, NH₄, NO₃, Organics and SO₄ measured by ACSM, and black carbon
298 measured with the aethalometer, are displayed in Figure 4. Each species exhibits different
299 temporal variations and concentration levels. Chloride is a minor fraction of PM₁ and its
300 concentration is lower than 3 $\mu\text{g m}^{-3}$ over the entire observation period. NH₄ is relatively
301 constant throughout the whole year at levels lower than 5 $\mu\text{g m}^{-3}$, with the exception of spring
302 2014 (March-May) where levels up to 15 $\mu\text{g m}^{-3}$ were observed. NO₃, Organics, SO₄ and BC
303 are much more time-dependent, with concentrations rising to 30-50 $\mu\text{g m}^{-3}$.
304 Some PM₁ species seem to exhibit significant seasonal variations (Figure S4, section D of the
305 SI; and Table 1). Average seasonal chloride concentrations were very low ($< 0.1 \mu\text{g m}^{-3}$).

306 Sulfates did not exhibit seasonal variations due to its industrial origin and showed similar
307 contributions from this sector (wind occurrences) for all seasons. Nevertheless, the NWR plot
308 (section E of the SI, Figure S5a) for sulfate shows a strong contribution from local sources,
309 highlighting the industrial sector, and a minor one from the marine sector, which could be the
310 result of ship emissions. This pattern is even more pronounced for its precursor SO₂ (Figure
311 S5b) whose high concentrations are clearly pointing at the industrial area. For the other
312 species, PM₁ measured during both summers 2013 and 2014 exhibit similar chemical
313 compositions due to similar wind patterns, which in turn likely imply the impact of similar
314 sources on the measurement site. However, the relative contribution of NO₃ is higher during
315 cold seasons (autumn, winter and spring) compared to the two warmer summers (Table 1).
316 Especially in spring 2014, NO₃ exhibits the highest average concentration (4 µg m⁻³) and
317 contribution (33%) when NH₃ emissions – required for the formation of ammonium nitrate –
318 start to peak in North-Western Europe due to fertilizer spreading. Besides, whereas 96% of
319 NH₃ emissions is attributed to the agricultural sector when considering the entire Hauts-de-
320 France region, it decreases down to 50% in the Dunkirk area, where local emissions from the
321 “manufacturing industries, waste treatment and construction” account for half according to
322 the latest available inventory (AtmoHdF 2012). The levels of ammonium and nitrate could
323 indeed be related to both a local and regional origin through their NWR plots (section E of the
324 SI, Figure S5c and d). The regional influence was further investigated through Concentration-
325 Weighted Trajectory (CWT) maps (section E of the SI, Figure S6), and pointed out a
326 significant contribution from medium- to long-range transport of aged ammonium nitrate
327 aerosols or their precursors from Central Europe (Germany, Poland, and Austria) (Figure S5).
328 Organics concentrations and contributions are also higher during cold seasons (autumn and
329 winter), which seems due to both local and regional sources (Figure S5e) coming from the
330 industrial-urban sector (55-63% of wind occurrences), such as emissions from urban sources
331 such as residential heating and traffic, while an additional contribution from industrial
332 emissions in this direction (storage facility of petrochemical products and food processing
333 industries) cannot be excluded. BC represents 5 to 9% of PM₁ mass but no clear observation
334 is found for its seasonal variation.

335 For the sake of comparison with other studies, Figure 5 displays 17 field campaigns
336 performed worldwide to investigate the composition of ambient aerosols. These studies
337 employed ACSM instruments in different environments classified as urban (5 sites), suburban
338 (2 sites), industrial-urban (2 sites) and rural (8 sites). For similar types of sites the studies are
339 sorted by decreasing NR-PM₁ mass concentrations. The durations of these campaigns are

340 highly variable and range from 3 weeks to 7 years. Campaigns performed on a timescale of
341 years can provide seasonal and even annual variations of submicron aerosols. The averaged
342 mass concentration varies from approximately 2-6 $\mu\text{g m}^{-3}$ for background sites (Hyytiälä,
343 Montsec, Look Rock) (Budisulistiorini et al. 2015, Minguillón et al. 2015, Heikkinen et al.
344 2020) up to 30-50 $\mu\text{g m}^{-3}$ for polluted cities (Santiago, Beijing) (Sun et al. 2012, Carbone et
345 al. 2013). Our study indicates an annual concentration of 9.0 $\mu\text{g m}^{-3}$, which is similar to that
346 observed for another industrial-urban site in Atlanta (9.5 $\mu\text{g m}^{-3}$) (Budisulistiorini et al.
347 2015), whose duration was one year.

348 The contribution of each species to NR-PM₁ is shown in the bottom panel of Figure 5.
349 Organics dominate (> 50%) for most of the sites and the contribution can reach up to 70% as
350 seen in Atlanta. In our study, organics account for 32% on average, which is within the lowest
351 contributions observed worldwide and similar to that found at the SIRTA suburban site near
352 Paris (39%) (Petit et al. 2015). Ammonium exhibits a relatively constant fraction at all
353 locations, with an average value of approximately 12%. The sulfate component contributes
354 from 8 to 35% of NR-PM₁, with higher contributions found for rural sites without (Tibetan
355 Plateau: 30%; South Africa: 32%) (Tiitta et al. 2014, Du et al. 2015) or with urban influence
356 (Senegal: 35%) (Rivellini et al. 2017). Interestingly, industrial sites do not exhibit the highest
357 levels of sulfate, whose contribution to the chemical composition does not seem to depend on
358 the nature of the site. Nitrate varies from 6% to 28%, with the highest values observed for
359 Paris (28%) (Petit et al. 2015), Dunkirk (26%) (this work) and Beijing (25%) (Sun et al.
360 2012). Higher levels of NO_x (NO and NO₂) in urban areas are likely the cause for higher
361 nitrate levels in PM₁ since NO_x are oxidized to nitric acid in the atmosphere, which in turn
362 forms secondary nitrate particles (Matsumoto and Tanaka 1996). Chloride is always a minor
363 fraction and represents less than 3% at all sites.

364 Figure 6 shows PM₁ mass concentrations and chemical compositions averaged over the entire
365 campaign for the four wind sectors defined above (marine, urban, industrial and industrial-
366 urban). The average concentration for all sectors is $9.4 \pm 9.1 \mu\text{g m}^{-3}$ with significantly higher
367 concentrations for the industrial ($11.7 \pm 8.8 \mu\text{g m}^{-3}$) and urban ($15.6 \pm 9.5 \mu\text{g m}^{-3}$) sectors, and
368 a lower concentration for the marine sector ($8.0 \pm 8.5 \mu\text{g m}^{-3}$). The organic fraction
369 contributes from 28% up to 38% of the PM₁, with the exception of the industrial sector for
370 which the aerosol composition is enriched in sulfate (only 14% organics). As mentioned
371 before, a higher organic fraction for the industrial-urban sector could be due to a storage
372 facility of petrochemical products or food processing industries in this area. For inorganic
373 species, the ammonium contribution is similar between all sectors ($\approx 14\%$) and non-refractory

374 chloride (therefore non-marine) represents less than 1% of the mass concentration. For
375 chloride, the small but significantly higher contribution from the industrial sector reflects the
376 presence of sources already identified in other campaigns in this area or similar ones (Hleis et
377 al. 2013, Taiwo et al. 2014, Crenn et al. 2017, Setyan et al. 2019), e.g. the formation of KCl in
378 the steelwork sintering process. Nitrate and sulfate contributions are more variable between
379 the different sectors, with contributions ranging from 8-35% for NO₃ and 13-58% for SO₄.
380 The urban and industrial sectors stand out by exhibiting the highest contributions for nitrate
381 (about 35%) and sulfates (about 58%), respectively. As mentioned previously, these higher
382 contributions may be due to higher NO_x and SO₂ emissions in the urban and industrial sectors,
383 respectively. BC contributes about 5% for the marine and industrial sectors, while it reaches 8
384 to 9% for the urban and industrial-urban sectors where traffic and wood burning may be
385 significant sources.

386

387 **3.3 Aerosol ion balance**

388 To investigate the ion balance of the sampled aerosols, a predicted concentration of NH₄ was
389 calculated from the sum of chloride, nitrate and sulfate ion concentrations using Eq. (2).
390 These ions are assumed to be bound to ammonium in a neutral aerosol to form NH₄Cl,
391 NH₄NO₃ and (NH₄)₂SO₄, respectively. The calculated value (NH_{4,predicted}) is then compared to
392 the measured NH₄ concentration. If the two values are similar, the particles are fully
393 neutralized. Although an ion balance cannot be used as a direct measurement of pH in
394 aerosols, it can still be used to distinguish qualitatively between an “acidic” (negative balance;
395 below the 1:1 line) and an “alkaline” (positive balance; above the 1:1 line) aerosol (Zhang et
396 al. 2007, Guo et al. 2015).

397 Particles are considered “more acidic” if the measured concentration is lower than the
398 predicted value, since the imbalance indicates that acidic compounds such as H₂SO₄, HNO₃ or
399 HCl are likely present in the aerosol. Note that as Cl being a minor fraction (<1%) of NR-
400 PM₁, the contribution of HCl to the aerosol ion balance – if present – is negligible.

401 Figure 7 displays the correlation between measured and predicted NH₄ with a color coding
402 based on SO₄ concentrations. All SO₄ concentrations higher than 25 μg m⁻³ are included in the
403 red color. When the symbols are scattered around the 1:1 line, the measured and predicted
404 concentrations are in good agreement, indicating that particulate ammonium is fully
405 neutralized. When the symbols are significantly below the 1:1 line, there is an overestimation
406 of the predicted concentrations. As mentioned above, this overestimation may be due to either

407 a lack of ammonium (thus of NH_3) or the presence of acidic species in the particles, which
408 may be characteristic of "fresh" emissions.

409 Aerosols appear not neutralized or "acidic" (below the 1:1 line) with high sulfate
410 concentrations (Figure 7a) but not with high nitrate concentrations (Figure S7, section F of the
411 SI). This observation suggests that aerosol ion balance is driven by acidic sulfate compounds.
412 The same analysis is displayed for the four wind sectors in Figure 7b-e. For the marine and
413 urban sectors, the aerosols are well neutralized and SO_4 concentrations are low ($4\text{-}5 \mu\text{g m}^{-3}$ on
414 average). NH_4 is therefore mainly bound to NO_3 . The industrial sector shows strong
415 deviations from the 1:1 line, with higher acidity levels correlated to elevated SO_4
416 concentrations (Figure 7e), which suggests that acidic aerosols are due to "fresh" industrial
417 emissions of sulfur compounds. It is interesting to note that the industrial-urban sector shows
418 a mixed behavior between industrial and urban sectors.

419 In order to investigate the influence of acidity on the NR- PM_1 composition, the measured-to-
420 predicted NH_4 ratio was plotted as box plots for the entire campaign and the four sectors in
421 Figure 8a. The aerosol composition for acidic and non-acidic particles is displayed in Figure
422 8b. Figure 8a clearly shows that the industrial sector exhibits the lowest $\text{NH}_{4,\text{measured-to-}}$
423 $\text{NH}_{4,\text{predicted}}$ ratio (0.64 on average), corresponding to the most acidic particles (ratio threshold
424 of 0.75). This ratio can be seen as a rough indicator of an equal number of moles of
425 $(\text{NH}_4)_2\text{SO}_4$ and NH_4HSO_4 (Zhang et al. 2005). The neutralized particles were defined for a
426 ratio ranging from the mean value of 0.85 to the 90th percentile (1.07). The "most acidic" and
427 "neutralized" periods account for 22% and 41% of the total sampling time, respectively. The
428 rest of the observations falls into a mildly acidic regime and are not analyzed separately.
429 Figure 8b displays the average composition of "neutralized" and "most acidic" particles,
430 respectively. Compared to those considered as neutralized, the "most acidic" particles
431 represent only half the mass. However, they contain more SO_4 (58% compared to 17%),
432 which is consistent with the above discussion. The acidic particles contain less nitrate (7%
433 compared to 34%), probably due to the displacement of HNO_3 by H_2SO_4 in the competition
434 for NH_3 (West et al. 1999).

435

436 **3.4 SO_2 -to- SO_4 conversion**

437 In the absence of direct measurements of industrial emissions, it is likely that some of the
438 particulate sulfate is directly produced during industrial processes, in particular as by-products
439 of the coke oven used to feed the three blast furnaces of the main steelworks in the area.
440 Furthermore, NH_4HSO_4 could be formed at the exit of the chimneys through the direct

441 reaction of SO_3 with H_2O and NH_3 in the presence of additional molecules (Chen et al. 2018).
442 Then NH_4HSO_4 can quickly react with NH_3 and form ammonium sulfate. However, a rapid
443 conversion of gaseous SO_2 into particulate sulfate could also contribute to the large sulfate
444 concentrations observed at the measurement site when the wind originates from the industrial
445 sector. The conversion can take place both in the gas phase (Stockwell and Calvert 1983,
446 Atkinson and Lloyd 1984) through an oxidation of SO_2 initiated by OH radicals, and in the
447 aqueous phase through reactions involving H_2O_2 and O_3 (Jacob and Hoffmann 1983,
448 Schwartz 1987). The sulfuric acid thus generated has a strong ability to nucleate in the
449 presence of water molecules and to form new particles by condensation of other low volatility
450 species (Kulmala et al. 2000, Weber et al. 2001). However, the oxidation of SO_2 in aqueous
451 phase is faster than in the gas-phase (Khoder 2002). Eatough et al. (1994) found that the gas-
452 phase oxidation rate can vary from <1% to 10% of ambient SO_2 per hour at high temperature
453 and relative humidity. Meanwhile, in the aqueous-phase the rate can reach 100% of SO_2
454 converted in less than an hour under optimum conditions (Eatough et al. 1994). Other
455 pathways such as the heterogeneous oxidation of S(IV) catalyzed by Fe(III) or Mn(II) (Jacob
456 and Hoffmann 1983) can occur, especially in this area where heavy metals have been
457 evidenced as important tracers of industrial emissions (Alleman et al. 2010, Setyan et al.
458 2019): When sulfuric acid is formed within or transferred to the aerosol, it reacts easily with
459 gaseous ammonia to form ammonium sulfate at the particle surface (Matsumoto and Tanaka
460 1996).

461 The observation of industrial plumes arriving at our ground sampling site requires that two
462 simultaneous conditions are met: (i) wind blowing from the southwest (industrial direction);
463 (ii) unstable atmospheric conditions favoring the dispersion of the plume. The Non-parametric
464 Wind Regression (NWR) plots of gaseous SO_2 and particulate SO_4 (Figure S6, a and b)
465 confirm that high concentrations observed at the receptor site are mainly originating from the
466 industrial sector (226° - 270°). Similar results were observed by a recent study near steel
467 plants in China, which showed important increases in sulfate, ammonium, CO and SO_2 when
468 industrial plumes reached the sampling site (Lei et al. 2020).

469 To assess whether the conversion of SO_2 into SO_4 was of importance during this study, the
470 influence of several microphysical and meteorological parameters on SO_2 , SO_4 and the
471 particulate sulfur fraction has been investigated. These parameters included atmospheric
472 vertical turbulences via the standard deviation σ_w of vertical wind speed w , horizontal wind
473 speed, relative humidity and temperature.

474 We defined the particulate sulfur fraction as the ratio of particulate sulfur to total sulfur
475 (S_p/S_{tot}), which is calculated as:

$$476 \quad \frac{S_p}{S_{tot}} = \frac{[SO_4] \times \frac{32}{96}}{[SO_2] \times \frac{32}{64} + [SO_4] \times \frac{32}{96}} \quad (4)$$

477 S_p/S_{tot} only takes into account the sulfur content and is not influenced by the oxygen content.

478 Two key parameters (RH and vertical turbulence) were found to significantly influence the
479 gas-particle partitioning of sulfur as shown in Figure 9 (left and right, respectively). SO_2 and
480 SO_4 concentrations, as well as S_p/S_{tot} ratios, shown in this figure are only considered within
481 the industrial sector to focus on the SO_2 -to- SO_4 conversion that occurs on a short timescale
482 (4-30 min) during the transport of fresh industrial emissions of sulfur compounds to the
483 sampling site. This data was binned accordingly to the descriptive parameter (RH, σ_w) with
484 the number of observations for each bin shown at the top of the first panel.

485 Figure 9a shows that SO_2 increases linearly with relative humidity until 70-80%. This
486 concomitant increase in RH and SO_2 could be due to industrial plumes passing over the
487 measurement site since these plumes are likely emitted with large concentrations of both
488 water and SO_2 . Interestingly, the SO_2 concentration starts decreasing when RH is higher than
489 80%, but an opposite trend is observed for SO_4 (Figure 9b). Indeed, SO_4 also increases with
490 RH until 80% but does not decrease for higher humidity levels. This behavior could be related
491 to a higher rate of SO_2 conversion at high humidity. In Figure 9c, the S_p/S_{tot} ratio clearly
492 shows that the particulate sulfur fraction is almost constant (approximately 0.1 with a low
493 level of dispersion in the values) for low RH conditions (RH < 70%). However, the sulfur
494 content is shifted from the gaseous to the particulate phase when RH is higher than 70-80%
495 (S_p/S_{tot} increases to 0.3 at 90-100% RH). This is likely due to the gas-particle conversion that
496 is favored under high RH conditions when the fast aqueous phase oxidation dominates. Sun et
497 al. reported a similar impact of RH on sulfate aerosols in Beijing for the winter season (Sun et
498 al. 2013). The authors showed that the average SO_4 -to-total sulfur ratio is less than 0.05 at low
499 RH (< 40%), indicating a very low sulfur oxidation ratio. This ratio quickly increases and
500 reaches 0.23 at high RH (80-90%). Recently, Zhao et al. studied the conversion of SO_2 into
501 sulfates on soot surfaces and found that water promotes sulfate formation for RH ranging
502 from 6%–70%, while RH > 80% inhibits it (Zhao et al. 2017). This trend was not observed
503 here because BC is only a minor contributor (~7%) of PM_{10} .

504 The atmospheric vertical turbulence can be characterized by the standard deviation σ_w of the
505 vertical wind speed w . This metric represents the fluctuation of vertical wind speed in units of
506 $m s^{-1}$ and quantifies the vertical mixing of air masses within the surface layer. Trends in SO_2 ,

507 SO₄ and S_p/S_{tot} on this parameter are shown in Figure 9 (right). For both SO₂ and SO₄, higher
508 σ_w values lead to higher concentrations (Figure 9a-b). As previously discussed, this can be
509 explained by elevated emission sources such as plumes from industrial chimneys, which can
510 reach the ground surface after dispersion only with strong enough vertical mixing. This
511 behavior had already been observed for some VOCs at the same site (Xiang et al. 2012). In
512 contrast, S_p/S_{tot} decreases with σ_w (Figure 9c), which suggests that the SO₂-to-SO₄ conversion
513 is less favored under highly turbulent conditions.

514 To better understand the multi-influence of humidity and vertical turbulence (σ_w) on the
515 conversion process, the examination of the RH dependence of the S_p/S_{tot} ratio was carried out
516 using four bins of σ_w (0-0.5, 0.5-1, 1-1.5 and ≥ 1.5 m s⁻¹) (Figure S7). This shows that the
517 S_p/S_{tot} ratio increases significantly with RH for each σ_w bin, except for the last one ($\sigma_w \geq 1.5$
518 m s⁻¹) where the change is unclear. Interestingly, higher conversion ratios seem to be observed
519 for low values of σ_w , which may be due to lower wind speed values, and as a consequence,
520 longer conversion times between the emission source and the measurement site. These results
521 indicate that high RH (> 70%) and relatively low σ_w values (< 1 m s⁻¹) are the best conditions
522 for an efficient SO₂-to-SO₄ conversion at this site.

523

524 **4 Conclusions**

525 The first long-term and near real-time measurements of the chemical composition of
526 submicron aerosols at an urban background and coastal site impacted by industrial emissions
527 showed a unique chemical signature compared to previous datasets existing in the literature.
528 The aerosol evolution and processing are tightly linked with meteorology and even
529 micrometeorology due to the complex dynamics of coastal areas, and the industrial emissions
530 at various stack heights. The complete dataset has been analyzed according to the season and
531 four different wind sectors. The aerosol ion balance based on measured and predicted NH₄
532 suggests that the majority of the particles are neutralized in the marine and urban sectors,
533 whereas in the industrial sector, “more acidic” particles generally contain significantly higher
534 concentrations of sulfate (~60%). Gas-phase SO₂ is strongly emitted in the nearby industrial
535 area and quickly processed to form secondary SO₄ particles on a timescale shorter than 30
536 min. Both SO₂ and SO₄ were mostly emitted by chimneys and therefore influenced by
537 atmospheric vertical mixing. High RH (>70%) and relatively low σ_w values (< 1 m s⁻¹)
538 provided the best conditions for an efficient SO₂-to-SO₄ conversion rate.

539

540 **Acknowledgements**

541 IMT Lille Douai and LPCA acknowledge financial support from the CaPPA (Chemical and
542 Physical Properties of the Atmosphere) project funded by the French National Research
543 Agency (ANR) through the PIA (Programme d'Investissement d'Avenir) under contract ANR-
544 11-LABX-0005-01, and two CPER projects funded by the French Ministry of Higher
545 Education and Research, the CNRS, the Regional Council "Hauts-de-France" and the
546 European Regional Development Fund (ERDF): Climibio, and IRENI (additionally financed
547 by the Communauté Urbaine de Dunkerque). We thank P. Goloub (LOA, Univ. Lille) for his
548 efforts in establishing and maintaining the PHOTONS/AERONET network, and L. Paringaux
549 (Atmo HdF) for technical support throughout the campaign. S. Zhang thanks IMT Lille Douai
550 and the Regional Council "Hauts-de-France" for her PhD grant. A. Chakraborty (IMT Lille
551 Douai) is acknowledged for helpful discussions.

552

553 **References**

- 554 Alfarra, M. R., H. Coe, J. D. Allan, K. N. Bower, H. Boudries, M. R. Canagaratna, J. L.
555 Jimenez, J. T. Jayne, A. A. Garforth, S.-M. Li and D. R. Worsnop (2004). "Characterization
556 of urban and rural organic particulate in the Lower Fraser Valley using two Aerodyne Aerosol
557 Mass Spectrometers." *Atmospheric Environment* **38**(34): 5745-5758.
- 558 Allan, J. D., A. E. Delia, H. Coe, K. N. Bower, M. R. Alfarra, J. L. Jimenez, A. M.
559 Middlebrook, F. Drewnick, T. B. Onasch, M. R. Canagaratna, J. T. Jayne and D. R. Worsnop
560 (2004). "A generalised method for the extraction of chemically resolved mass spectra from
561 Aerodyne aerosol mass spectrometer data." *Journal of Aerosol Science* **35**(7): 909-922.
- 562 Alleman, L. Y., L. Lamaison, E. Perdrix, A. Robache and J.-C. Galloo (2010). "PM10 metal
563 concentrations and source identification using positive matrix factorization and wind
564 sectoring in a French industrial zone." *Atmospheric Research* **96**(4): 612-625.
- 565 Atkinson, R. and A. C. Lloyd (1984). "Evaluation of Kinetic and Mechanistic Data for
566 Modeling of Photochemical Smog." *Journal of Physical and Chemical Reference Data* **13**(2):
567 315-444.
- 568 AtmoHdF (2012). Inventaire régional des émissions de polluants atmosphériques, Atmo
569 Hauts-de-France.
- 570 Badol, C., N. Locoge and J.-C. Galloo (2008). "Using a source-receptor approach to
571 characterise VOC behaviour in a French urban area influenced by industrial emissions: Part
572 II: Source contribution assessment using the Chemical Mass Balance (CMB) model." *Science
573 of The Total Environment* **389**(2-3): 429-440.
- 574 Badol, C., N. Locoge, T. Léonardis and J.-C. Galloo (2008). "Using a source-receptor
575 approach to characterise VOC behaviour in a French urban area influenced by industrial
576 emissions Part I: Study area description, data set acquisition and qualitative data analysis of
577 the data set." *Science of The Total Environment* **389**(2-3): 441-452.
- 578 Boichu, M., O. Favez, V. Riffault, J. E. Petit, Y. Zhang, C. Brogniez, J. Sciare, I. Chiapello,
579 L. Clarisse, S. Zhang, N. Pujol-Söhne, E. Tison, H. Delbarre and P. Goloub (2019). "Large-
580 scale particulate air pollution and chemical fingerprint of volcanic sulfate aerosols from the

581 2014–2015 Holuhraun flood lava eruption of Bárðarbunga volcano (Iceland)." Atmos. Chem.
582 Phys. **19**(22): 14253-14287.

583 Bouwman, A. F., D. P. Van Vuuren, R. G. Derwent and M. Posch (2002). "A Global Analysis
584 of Acidification and Eutrophication of Terrestrial Ecosystems." Water, Air, and Soil Pollution
585 **141**(1): 349-382.

586 Budisulistiorini, S. H., K. Baumann, E. S. Edgerton, S. T. Bairai, S. Mueller, S. L. Shaw, E.
587 M. Knipping, A. Gold and J. D. Surratt (2015). "Seasonal characterization of submicron
588 aerosol chemical composition and organic aerosol sources in the southeastern United States:
589 Atlanta, Georgia and Look Rock, Tennessee." Atmos. Chem. Phys. Discuss. **15**(16): 22379-
590 22417.

591 Canagaratna, M. R., J. T. Jayne, J. L. Jimenez, J. D. Allan, M. R. Alfarra, Q. Zhang, T. B.
592 Onasch, F. Drewnick, H. Coe, A. Middlebrook, A. Delia, L. R. Williams, A. M. Trimborn, M.
593 J. Northway, P. F. DeCarlo, C. E. Kolb, P. Davidovits and D. R. Worsnop (2007). "Chemical
594 and microphysical characterization of ambient aerosols with the aerodyne aerosol mass
595 spectrometer." Mass Spectrometry Reviews **26**(2): 185-222.

596 Carbone, S., S. Saarikoski, A. Frey, F. Reyes, P. Reyes, M. Castillo, E. Gramsch, P. Oyola, J.
597 Jayne, D. R. Worsnop and R. Hillamo (2013). "Chemical Characterization of Submicron
598 Aerosol Particles in Santiago de Chile." Aerosol and Air Quality Research **13**.

599 Cazier, F., D. Dewaele, A. Delbende, H. Nouali, G. Garçon, A. Verdin, D. Courcot, S.
600 Bouhsina and P. Shirali (2011). "Sampling analysis and characterization of particles in the
601 atmosphere of rural, urban and industrial areas." Procedia Environmental Sciences **4**(0): 218-
602 227.

603 CGDD (2014). Bilan de la qualité de l'air en France en 2013, Commissariat général au
604 développement durable.

605 Chen, S., Y. Zhao and R. Zhang (2018). "Formation Mechanism of Atmospheric Ammonium
606 Bisulfate: Hydrogen-Bond-Promoted Nearly Barrierless Reactions of SO₃ with NH₃ and
607 H₂O." **19**(8): 967-972.

608 Cohen, A. J., H. Ross Anderson, B. Ostro, K. D. Pandey, M. Krzyzanowski, N. Kunzli, K.
609 Gutschmidt, A. Pope, I. Romieu, J. M. Samet and K. Smith (2005). "The global burden of
610 disease due to outdoor air pollution." J Toxicol Environ Health A **68**(13-14): 1301-1307.

611 Crenn, V., A. Chakraborty, I. Fronval, D. Petitprez and V. Riffault (2018). "Fine particles
612 sampled at an urban background site and an industrialized coastal site in Northern France—
613 Part 2: Comparison of offline and online analyses for carbonaceous aerosols." Aerosol
614 Science and Technology **52**(3): 287-299.

615 Crenn, V., I. Fronval, D. Petitprez and V. Riffault (2017). "Fine particles sampled at an urban
616 background site and an industrialized coastal site in Northern France - Part 1: Seasonal
617 variations and chemical characterization." Sci Total Environ **578**: 203-218.

618 Crenn, V., J. Sciare, P. L. Croteau, S. Verlhac, R. Fröhlich, C. A. Belis, W. Aas, M. Äijälä, A.
619 Alastuey, B. Artiñano, D. Baisnée, N. Bonnaire, M. Bressi, M. Canagaratna, F. Canonaco, C.
620 Carbone, F. Cavalli, E. Coz, M. J. Cubison, J. K. Esser-Gietl, D. C. Green, V. Gros, L.
621 Heikkinen, H. Herrmann, C. Lunder, M. C. Minguillón, G. Močnik, C. D. O'Dowd, J.
622 Ovadnevaite, J. E. Petit, E. Petralia, L. Poulain, M. Priestman, V. Riffault, A. Ripoll, R.
623 Sarda-Estève, J. G. Slowik, A. Setyan, A. Wiedensohler, U. Baltensperger, A. S. H. Prévôt, J.
624 T. Jayne and O. Favez (2015). "ACTRIS ACSM intercomparison – Part 1: Reproducibility of
625 concentration and fragment results from 13 individual Quadrupole Aerosol Chemical

626 Speciation Monitors (Q-ACSM) and consistency with co-located instruments." Atmos. Meas.
627 Tech. **8**(12): 5063-5087.

628 DeCarlo, P. F., J. R. Kimmel, A. Trimborn, M. J. Northway, J. T. Jayne, A. C. Aiken, M.
629 Gonin, K. Fuhrer, T. Horvath, K. S. Docherty, D. R. Worsnop and J. L. Jimenez (2006).
630 "Field-Deployable, High-Resolution, Time-of-Flight Aerosol Mass Spectrometer." Analytical
631 Chemistry **78**(24): 8281-8289.

632 DREAL (2012). Industrie au regard de l'environnement, Direction régionale de
633 l'environnement de l'aménagement et du logement Nord-Pas-de-Calais: 11-25.

634 Du, W., Y. L. Sun, Y. S. Xu, Q. Jiang, Q. Q. Wang, W. Yang, F. Wang, Z. P. Bai, X. D. Zhao
635 and Y. C. Yang (2015). "Chemical characterization of submicron aerosol and particle growth
636 events at a national background site (3295 m a.s.l.) on the Tibetan Plateau." Atmos. Chem.
637 Phys. **15**(18): 10811-10824.

638 Eatough, D. J., F. M. Caka and R. J. Farber (1994). "The Conversion of SO₂ to Sulfate in the
639 Atmosphere." Israel Journal of Chemistry **34**(3-4): 301-314.

640 EEA (2015). Sector share for emissions of primary PM_{2.5} and PM₁₀ particulate matter,
641 European Environment Agency: [http://www.eea.europa.eu/data-and-maps/daviz/sector-split-](http://www.eea.europa.eu/data-and-maps/daviz/sector-split-of-emissions-of-4#tab-chart_1)
642 [of-emissions-of-4#tab-chart_1](http://www.eea.europa.eu/data-and-maps/daviz/sector-split-of-emissions-of-4#tab-chart_1).

643 El Haddad, I., B. D'Anna, B. Temime-Roussel, M. Nicolas, A. Boreave, O. Favez, D. Voisin,
644 J. Sciare, C. George, J. L. Jaffrezo, H. Wortham and N. Marchand (2013). "Towards a better
645 understanding of the origins, chemical composition and aging of oxygenated organic aerosols:
646 case study of a Mediterranean industrialized environment, Marseille." Atmos. Chem. Phys.
647 **13**(15): 7875-7894.

648 Elder, A., S. Vidyasagar and L. DeLouise (2009). "Physicochemical factors that affect metal
649 and metal oxide nanoparticle passage across epithelial barriers." Wiley Interdisciplinary
650 Reviews: Nanomedicine and Nanobiotechnology **1**(4): 434-450.

651 Flossmann, A. I., W. D. Hall and H. R. Pruppacher (1985). "A Theoretical Study of the Wet
652 Removal of Atmospheric Pollutants. Part I: The Redistribution of Aerosol Particles Captured
653 through Nucleation and Impaction Scavenging by Growing Cloud Drops." Journal of the
654 Atmospheric Sciences **42**(6): 583-606.

655 Ghan, S. J. and S. E. Schwartz (2007). "Aerosol Properties and Processes: A Path from Field
656 and Laboratory Measurements to Global Climate Models." Bulletin of the American
657 Meteorological Society **88**(7): 1059-1083.

658 Guo, H., L. Xu, A. Bougiatioti, K. M. Cerully, S. L. Capps, J. R. Hite Jr, A. G. Carlton, S. H.
659 Lee, M. H. Bergin, N. L. Ng, A. Nenes and R. J. Weber (2015). "Fine-particle water and pH
660 in the southeastern United States." Atmos. Chem. Phys. **15**(9): 5211-5228.

661 Heikkinen, L., M. Äijälä, M. Riva, K. Luoma, K. Dällenbach, J. Aalto, P. Aalto, D. Aliaga,
662 M. Aurela, H. Keskinen, U. Makkonen, P. Rantala, M. Kulmala, T. Petäjä, D. Worsnop and
663 M. Ehn (2020). "Long-term sub-micrometer aerosol chemical composition in the boreal
664 forest: inter- and intra-annual variability." Atmos. Chem. Phys. **20**(5): 3151-3180.

665 Hleis, D., I. Fernández-Olmo, F. Ledoux, A. Kfoury, L. Courcot, T. Desmonts and D. Courcot
666 (2013). "Chemical profile identification of fugitive and confined particle emissions from an
667 integrated iron and steelmaking plant." Journal of Hazardous Materials **250-251**: 246-255.

668 Jacob, D. J. and M. R. Hoffmann (1983). "A dynamic model for the production of H⁺ NO₃⁻,
669 and SO₄²⁻ in urban fog." Journal of Geophysical Research: Oceans **88**(C11): 6611-6621.

670 Jayne, J. T., D. C. Leard, X. Zhang, P. Davidovits, K. A. Smith, C. E. Kolb and D. R.
671 Worsnop (2000). "Development of an Aerosol Mass Spectrometer for Size and Composition
672 Analysis of Submicron Particles." Aerosol Science and Technology **33**(1-2): 49-70.

673 Jimenez, J. L., M. R. Canagaratna, N. M. Donahue, A. S. H. Prevot, Q. Zhang, J. H. Kroll, P.
674 F. DeCarlo, J. D. Allan, H. Coe, N. L. Ng, A. C. Aiken, K. S. Docherty, I. M. Ulbrich, A. P.
675 Grieshop, A. L. Robinson, J. Duplissy, J. D. Smith, K. R. Wilson, V. A. Lanz, C. Hueglin, Y.
676 L. Sun, J. Tian, A. Laaksonen, T. Raatikainen, J. Rautiainen, P. Vaattovaara, M. Ehn, M.
677 Kulmala, J. M. Tomlinson, D. R. Collins, M. J. Cubison, E., J. Dunlea, J. A. Huffman, T. B.
678 Onasch, M. R. Alfarra, P. I. Williams, K. Bower, Y. Kondo, J. Schneider, F. Drewnick, S.
679 Borrmann, S. Weimer, K. Demerjian, D. Salcedo, L. Cottrell, R. Griffin, A. Takami, T.
680 Miyoshi, S. Hatakeyama, A. Shimono, J. Y. Sun, Y. M. Zhang, K. Dzepina, J. R. Kimmel, D.
681 Sueper, J. T. Jayne, S. C. Herndon, A. M. Trimborn, L. R. Williams, E. C. Wood, A. M.
682 Middlebrook, C. E. Kolb, U. Baltensperger and D. R. Worsnop (2009). "Evolution of Organic
683 Aerosols in the Atmosphere." Science **326**(5959): 1525-1529.

684 Jimenez, J. L., J. T. Jayne, Q. Shi, C. E. Kolb, D. R. Worsnop, I. Yourshaw, J. H. Seinfeld, R.
685 C. Flagan, X. Zhang, K. A. Smith, J. W. Morris and P. Davidovits (2003). "Ambient aerosol
686 sampling using the Aerodyne Aerosol Mass Spectrometer." Journal of Geophysical Research:
687 Atmospheres **108**(D7).

688 Kelly, F. J. and J. C. Fussell (2012). "Size, source and chemical composition as determinants
689 of toxicity attributable to ambient particulate matter." Atmospheric Environment **60**: 504-526.

690 Khoder, M. I. (2002). "Atmospheric conversion of sulfur dioxide to particulate sulfate and
691 nitrogen dioxide to particulate nitrate and gaseous nitric acid in an urban area." Chemosphere
692 **49**(6): 675-684.

693 Kulmala, M., L. Pirjola and J. M. Makela (2000). "Stable sulphate clusters as a source of new
694 atmospheric particles." Nature **404**(6773): 66-69.

695 Leclercq, B., A. Platel, S. Antherieu, L. Y. Alleman, E. M. Hardy, E. Perdrix, N. Grova, V.
696 Riffault, B. M. Appenzeller, M. Happillon, F. Nessler, P. Coddeville, J. M. Lo-Guidice and
697 G. Garçon (2017). "Genetic and epigenetic alterations in normal and sensitive COPD-diseased
698 human bronchial epithelial cells repeatedly exposed to air pollution-derived PM_{2.5}." Environ
699 Pollut **230**: 163-177.

700 Lei, L., C. Xie, D. Wang, Y. He, Q. Wang, W. Zhou, W. Hu, P. Fu, Y. Chen, X. Pan, Z.
701 Wang, D. R. Worsnop and Y. Sun (2020). "Fine particle characterization in a coastal city in
702 China: composition, sources, and impacts of industrial emissions." Atmos. Chem. Phys.
703 **20**(5): 2877-2890.

704 Matsumoto, K. and H. Tanaka (1996). "Formation and dissociation of atmospheric particulate
705 nitrate and chloride: An approach based on phase equilibrium." Atmospheric Environment
706 **30**(4): 639-648.

707 Matthew, B. M., A. M. Middlebrook and T. B. Onasch (2008). "Collection Efficiencies in an
708 Aerodyne Aerosol Mass Spectrometer as a Function of Particle Phase for Laboratory
709 Generated Aerosols." Aerosol Science and Technology **42**(11): 884-898.

710 Mazzarella, G., V. Esposito, A. Bianco, F. Ferraraccio, M. V. Prati, A. Lucariello, L.
711 Manente, A. Mezzogiorno and A. De Luca (2012). "Inflammatory effects on human lung
712 epithelial cells after exposure to diesel exhaust micron sub particles (PM_{1.0}) and pollen
713 allergens." Environmental Pollution **161**: 64-69.

714 Mbengue, S., L. Y. Alleman and P. Flament (2014). "Size-distributed metallic elements in
715 submicronic and ultrafine atmospheric particles from urban and industrial areas in northern
716 France." Atmospheric Research **135–136**(0): 35-47.

717 Middlebrook, A. M., R. Bahreini, J. L. Jimenez and M. R. Canagaratna (2011). "Evaluation of
718 Composition-Dependent Collection Efficiencies for the Aerodyne Aerosol Mass Spectrometer
719 using Field Data." Aerosol Science and Technology **46**(3): 258-271.

720 Minguillón, M. C., A. Ripoll, N. Pérez, A. S. H. Prévôt, F. Canonaco, X. Querol and A.
721 Alastuey (2015). "Chemical characterization of submicron regional background aerosols in
722 the western Mediterranean using an Aerosol Chemical Speciation Monitor." Atmos. Chem.
723 Phys. **15**(11): 6379-6391.

724 Ng, N. L., S. C. Herndon, A. Trimborn, M. R. Canagaratna, P. L. Croteau, T. B. Onasch, D.
725 Sueper, D. R. Worsnop, Q. Zhang, Y. L. Sun and J. T. Jayne (2011). "An Aerosol Chemical
726 Speciation Monitor (ACSM) for Routine Monitoring of the Composition and Mass
727 Concentrations of Ambient Aerosol." Aerosol Science and Technology **45**(7): 780-794.

728 Niyogi, D., H.-I. Chang, V. K. Saxena, T. Holt, K. Alapaty, F. Booker, F. Chen, K. J. Davis,
729 B. Holben, T. Matsui, T. Meyers, W. C. Oechel, R. A. Pielke, R. Wells, K. Wilson and Y.
730 Xue (2004). "Direct observations of the effects of aerosol loading on net ecosystem CO₂
731 exchanges over different landscapes." Geophysical Research Letters **31**(20): L20506.

732 Park, S. S., A. D. A. Hansen and S. Y. Cho (2010). "Measurement of real time black carbon
733 for investigating spot loading effects of Aethalometer data." Atmospheric Environment
734 **44**(11): 1449-1455.

735 Parworth, C., J. Fast, F. Mei, T. Shippert, C. Sivaraman, A. Tilp, T. Watson and Q. Zhang
736 (2015). "Long-term measurements of submicrometer aerosol chemistry at the Southern Great
737 Plains (SGP) using an Aerosol Chemical Speciation Monitor (ACSM)." Atmospheric
738 Environment **106**: 43-55.

739 Pérez, N., J. Pey, X. Querol, A. Alastuey, J. M. López and M. Viana (2008). "Partitioning of
740 major and trace components in PM₁₀–PM_{2.5}–PM₁ at an urban site in Southern Europe."
741 Atmospheric Environment **42**(8): 1677-1691.

742 Petit, J. E., O. Favez, A. Albinet and F. Canonaco (2017). "A user-friendly tool for
743 comprehensive evaluation of the geographical origins of atmospheric pollution: Wind and
744 trajectory analyses." Environmental Modelling & Software **88**: 183-187.

745 Petit, J. E., O. Favez, J. Sciare, V. Cretnn, R. Sarda-Estève, N. Bonnaire, G. Močnik, J. C.
746 Dupont, M. Haeffelin and E. Leoz-Garziandia (2015). "Two years of near real-time chemical
747 composition of submicron aerosols in the region of Paris using an Aerosol Chemical
748 Speciation Monitor (ACSM) and a multi-wavelength Aethalometer." Atmos. Chem. Phys.
749 **15**(6): 2985-3005.

750 Petzold, A., C. Kopp and R. Niessner (1997). "The dependence of the specific attenuation
751 cross-section on black carbon mass fraction and particle size." Atmospheric Environment
752 **31**(5): 661-672.

753 Pope, C. A., R. T. Burnett, M. J. Thun and et al. (2002). "Lung cancer, cardiopulmonary
754 mortality, and long-term exposure to fine particulate air pollution." JAMA **287**(9): 1132-1141.

755 Ramgolam, K., O. Favez, H. Cachier, A. Gaudichet, F. Marano, L. Martinon and A. Baeza-
756 Squiban (2009). "Size-partitioning of an urban aerosol to identify particle determinants
757 involved in the proinflammatory response induced in airway epithelial cells." Part Fibre
758 Toxicol **6**: 10.

759 Riffault, V., J. Arndt, H. Marris, S. Mbengue, A. Setyan, L. Y. Alleman, K. Deboudt, P.
760 Flament, P. Augustin, H. Delbarre and J. Wenger (2015). "Fine and Ultrafine Particles in the
761 Vicinity of Industrial Activities: A Review." Critical Reviews in Environmental Science and
762 Technology: 1-52.

763 Rimetz-Planchon, J., E. Perdrix, S. Sobanska and C. Brémard (2008). "PM10 air quality
764 variations in an urbanized and industrialized harbor." Atmospheric Environment **42**(31):
765 7274-7283.

766 Ripoll, A., M. C. Minguillón, J. Pey, J. L. Jimenez, D. A. Day, Y. Sosedova, F. Canonaco, A.
767 S. H. Prévôt, X. Querol and A. Alastuey (2015). "Long-term real-time chemical
768 characterization of submicron aerosols at Montsec (southern Pyrenees, 1570 m a.s.l.)."
769 Atmos. Chem. Phys. **15**(6): 2935-2951.

770 Rivellini, L. H., I. Chiapello, E. Tison, M. Fourmentin, A. Féron, A. Diallo, T. N'Diaye, P.
771 Goloub, F. Canonaco, A. S. H. Prévôt and V. Riffault (2017). "Chemical characterization and
772 source apportionment of submicron aerosols measured in Senegal during the 2015 SHADOW
773 campaign." Atmos. Chem. Phys. **17**(17): 10291-10314.

774 Roig Rodelas, R., E. Perdrix, B. Herbin and V. Riffault (2019). "Characterization and
775 variability of inorganic aerosols and their gaseous precursors at a suburban site in northern
776 France over one year (2015–2016)." Atmospheric Environment **200**: 142-157.

777 Roukos, J., V. Riffault, N. Locoge and H. Plaisance (2009). "VOC in an urban and industrial
778 harbor on the French North Sea coast during two contrasted meteorological situations."
779 Environmental Pollution **157**(11): 3001-3009.

780 Schlag, P., A. Kiendler-Scharr, M. J. Blom, F. Canonaco, J. S. Henzing, M. M. Moerman, A.
781 S. H. Prévôt and R. Holzinger (2015). "Aerosol source apportionment from 1 year
782 measurements at the CESAR tower at Cabauw, NL." Atmos. Chem. Phys. Discuss. **2015**:
783 35117-35155.

784 Schwartz, S. E. (1987). Aqueous-Phase Reactions in Clouds. The Chemistry of Acid Rain,
785 American Chemical Society. **349**: 93-108.

786 Setyan, A., P. Flament, N. Locoge, K. Deboudt, V. Riffault, L. Y. Alleman, C. Schoemaeker,
787 J. Arndt, P. Augustin, R. M. Healy, J. C. Wenger, F. Cazier, H. Delbarre, D. Dewaele, P.
788 Dewalle, M. Fourmentin, P. Genevray, C. Gengembre, T. Leonardis, H. Marris and S.
789 Mbengue (2019). "Investigation on the near-field evolution of industrial plumes from
790 metalworking activities." Science of The Total Environment **668**: 443-456.

791 Stavroulas, I., A. Bougiatioti, G. Grivas, D. Paraskevopoulou, M. Tsagkaraki, P. Zarnpas, E.
792 Liakakou, E. Gerasopoulos and N. Mihalopoulos (2019). "Sources and processes that control
793 the submicron organic aerosol composition in an urban Mediterranean environment (Athens):
794 a high temporal-resolution chemical composition measurement study." Atmos. Chem. Phys.
795 **19**(2): 901-919.

796 Stein, A. F., R. R. Draxler, G. D. Rolph, B. J. B. Stunder, M. D. Cohen and F. Ngan (2016).
797 "NOAA's HYSPLIT Atmospheric Transport and Dispersion Modeling System." Bulletin of
798 the American Meteorological Society **96**(12): 2059-2077.

799 Stockwell, W. R. and J. G. Calvert (1983). "The mechanism of the HO-SO₂ reaction."
800 Atmospheric Environment (1967) **17**(11): 2231-2235.

801 Sun, Y., Z. Wang, H. Dong, T. Yang, J. Li, X. Pan, P. Chen and J. T. Jayne (2012).
802 "Characterization of summer organic and inorganic aerosols in Beijing, China with an
803 Aerosol Chemical Speciation Monitor." Atmospheric Environment **51**: 250-259.

804 Sun, Y., Z. Wang, P. Fu, Q. Jiang, T. Yang, J. Li and X. Ge (2013). "The impact of relative
805 humidity on aerosol composition and evolution processes during wintertime in Beijing,
806 China." Atmospheric Environment **77**: 927-934.

807 Taiwo, A. M., R. M. Harrison, D. C. S. Beddows and Z. Shi (2014). "Source apportionment of
808 single particles sampled at the industrially polluted town of Port Talbot, United Kingdom by
809 ATOFMS." Atmospheric Environment **97**: 155-165.

810 Taiwo, A. M., R. M. Harrison and Z. Shi (2014). "A review of receptor modelling of
811 industrially emitted particulate matter." Atmospheric Environment **97**: 109-120.

812 Takahama, S., A. Johnson, J. Guzman Morales, L. M. Russell, R. Duran, G. Rodriguez, J.
813 Zheng, R. Zhang, D. Toom-Saunty and W. R. Leitch (2013). "Submicron organic aerosol in
814 Tijuana, Mexico, from local and Southern California sources during the CalMex campaign."
815 Atmospheric Environment **70**: 500-512.

816 Tiitta, P., V. Vakkari, P. Croteau, J. P. Beukes, P. G. van Zyl, M. Josipovic, A. D. Venter, K.
817 Jaars, J. J. Pienaar, N. L. Ng, M. R. Canagaratna, J. T. Jayne, V. M. Kerminen, H. Kokkola,
818 M. Kulmala, A. Laaksonen, D. R. Worsnop and L. Laakso (2014). "Chemical composition,
819 main sources and temporal variability of PM1 aerosols in southern African grassland." Atmos.
820 Chem. Phys. **14**(4): 1909-1927.

821 Virkkula, A., T. Mäkelä, R. Hillamo, T. Yli-tuomi, A. Hirsikko, K. Hameri and I. k. Koponen
822 (2007). "A simple procedure for correcting loading effects of aethalometer data." Journal of
823 the Air & Waste Management Association **57**(10).

824 von der Weiden, S. L., F. Drewnick and S. Borrmann (2009). "Particle Loss Calculator – a
825 new software tool for the assessment of the performance of aerosol inlet systems." Atmos.
826 Meas. Tech. **2**(2): 479-494.

827 Weber, R. J., G. Chen, D. D. Davis, R. L. Mauldin, D. J. Tanner, F. L. Eisele, A. D. Clarke,
828 D. C. Thornton and A. R. Bandy (2001). "Measurements of enhanced H₂SO₄ and 3–4 nm
829 particles near a frontal cloud during the First Aerosol Characterization Experiment (ACE 1)."
830 Journal of Geophysical Research: Atmospheres **106**(D20): 24107-24117.

831 Weingartner, E., H. Saathoff, M. Schnaiter, N. Streit, B. Bitnar and U. Baltensperger (2003).
832 "Absorption of light by soot particles: determination of the absorption coefficient by means of
833 aethalometers." Journal of Aerosol Science **34**(10): 1445-1463.

834 West, J. J., A. S. Ansari and S. N. Pandis (1999). "Marginal PM_{2.5}: Nonlinear Aerosol Mass
835 Response to Sulfate Reductions in the Eastern United States." Journal of the Air & Waste
836 Management Association **49**(12): 1415-1424.

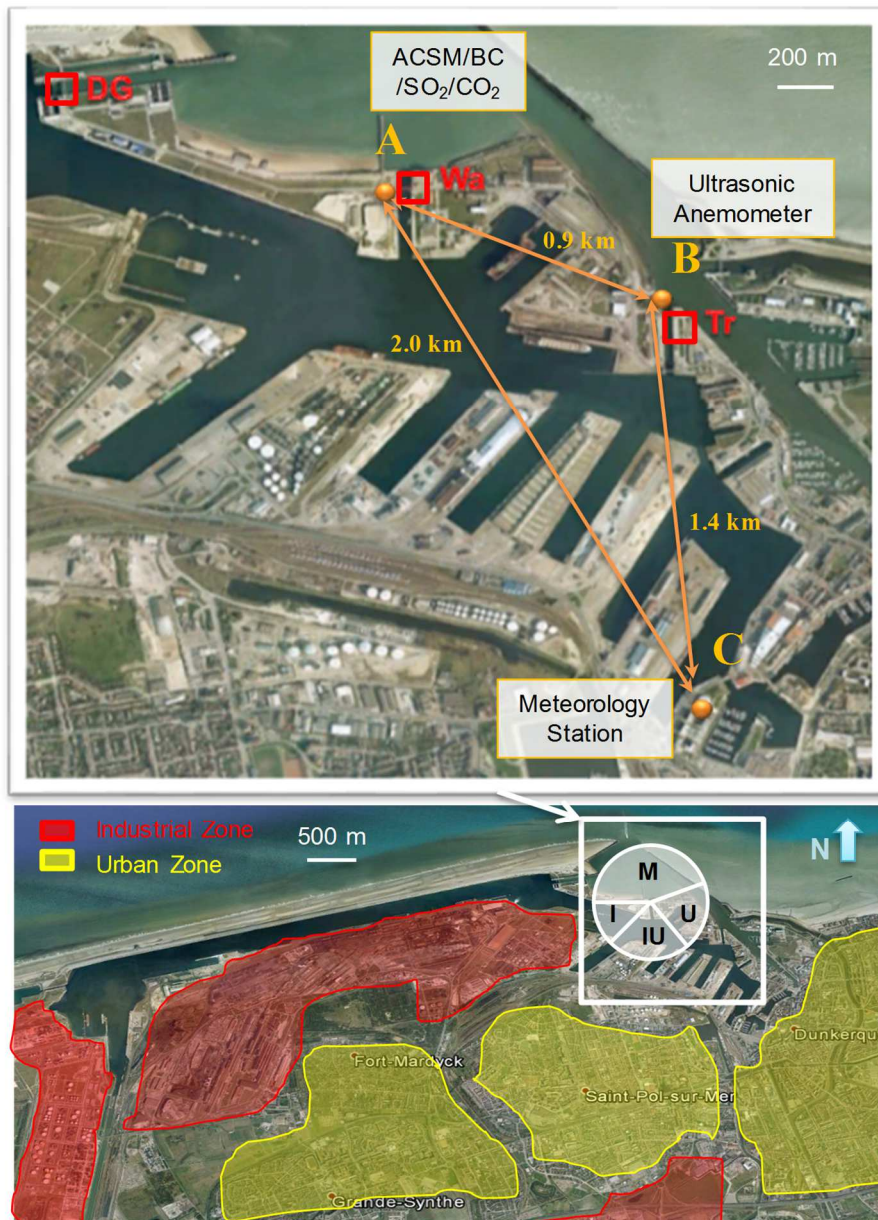
837 WHO (2002). The world health report 2002 - Reducing Risks, Promoting Healthy Life.
838 Geneva: http://www.who.int/whr/2002/en/whr2002_en.pdf?ua=2001.

839 Xiang, Y., H. Delbarre, S. Sauvage, T. Léonardis, M. Fourmentin, P. Augustin and N. Locoge
840 (2012). "Development of a methodology examining the behaviours of VOCs source
841 apportionment with micro-meteorology analysis in an urban and industrial area."
842 Environmental Pollution **162**: 15-28.

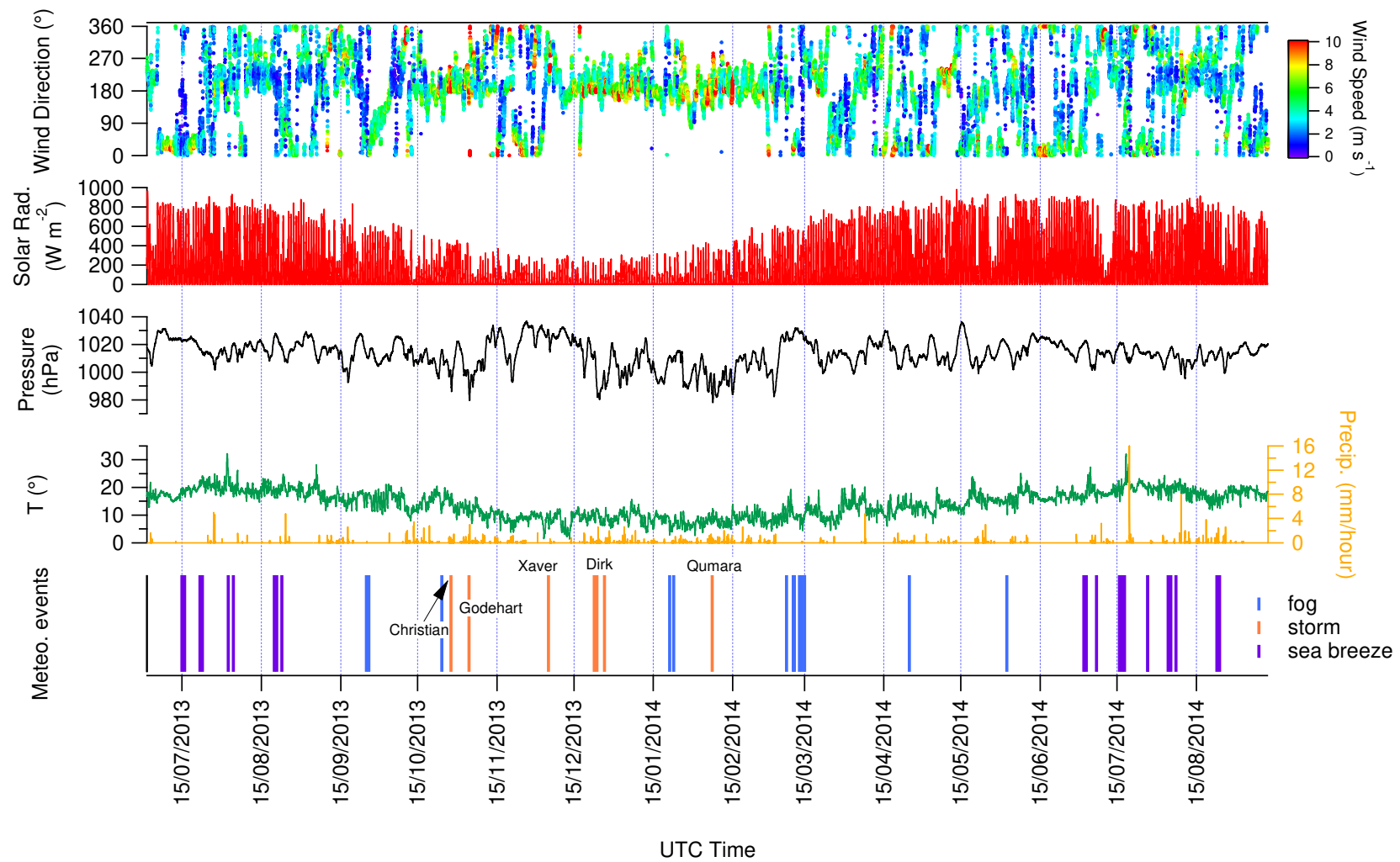
843 Zhang, Q., M. R. Canagaratna, J. T. Jayne, D. R. Worsnop and J.-L. Jimenez (2005). "Time-
844 and size-resolved chemical composition of submicron particles in Pittsburgh: Implications for
845 aerosol sources and processes." Journal of Geophysical Research: Atmospheres **110**(D7):
846 D07S09.

847 Zhang, Q., J. L. Jimenez, M. R. Canagaratna, J. D. Allan, H. Coe, I. Ulbrich, M. R. Alfarra,
848 A. Takami, A. M. Middlebrook, Y. L. Sun, K. Dzepina, E. Dunlea, K. Docherty, P. F.

- 849 DeCarlo, D. Salcedo, T. Onasch, J. T. Jayne, T. Miyoshi, A. Shimono, S. Hatakeyama, N.
850 Takegawa, Y. Kondo, J. Schneider, F. Drewnick, S. Borrmann, S. Weimer, K. Demerjian, P.
851 Williams, K. Bower, R. Bahreini, L. Cottrell, R. J. Griffin, J. Rautiainen, J. Y. Sun, Y. M.
852 Zhang and D. R. Worsnop (2007). "Ubiquity and dominance of oxygenated species in organic
853 aerosols in anthropogenically-influenced Northern Hemisphere midlatitudes." Geophysical
854 Research Letters **34**(13): L13801.
- 855 Zhang, Q., J. L. Jimenez, D. R. Worsnop and M. Canagaratna (2007). "A Case Study of
856 Urban Particle Acidity and Its Influence on Secondary Organic Aerosol." Environmental
857 Science & Technology **41**(9): 3213-3219.
- 858 Zhao, Y., Y. Liu, J. Ma, Q. Ma and H. He (2017). "Heterogeneous reaction of SO₂ with soot:
859 The roles of relative humidity and surface composition of soot in surface sulfate formation."
860 Atmospheric Environment **152**: 465-476.

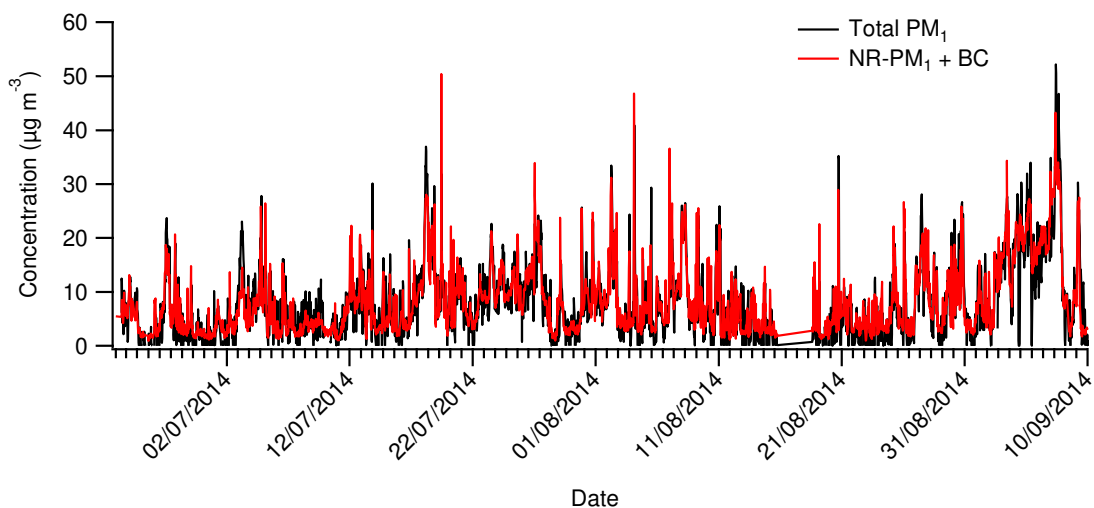


861
 862 Figure 1. (Bottom) Maps of the urban-industrial area of Dunkirk (M: marine, U: urban, IU:
 863 industrial-urban, I: industrial wind sectors); Top Locations of the measurements: (A) Port-Est:
 864 ACSM and other chemical measurements; (B) Ultrasonic anemometer; (C) Meteorology
 865 station. Locks indicated in red (DG: De Gaulle; Wa: Watier; Tr: Trystram) (adapted from
 866 Google Maps)

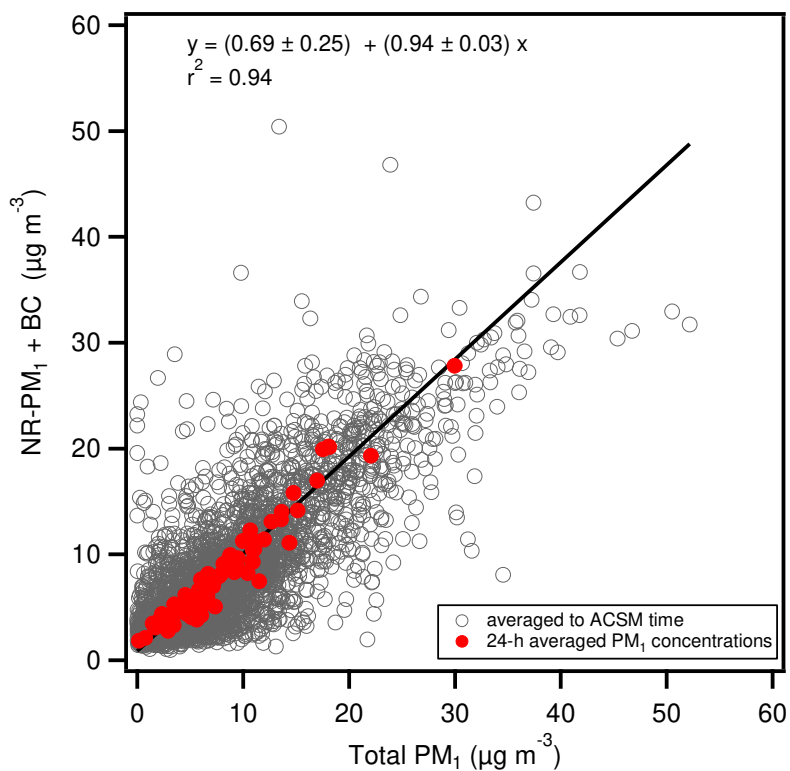


867

868 Figure 2. From top to bottom: wind direction colored by wind speed, solar radiation, pressure, temperature and precipitation, and identified
 869 meteorological events (fog, storm and sea breeze).

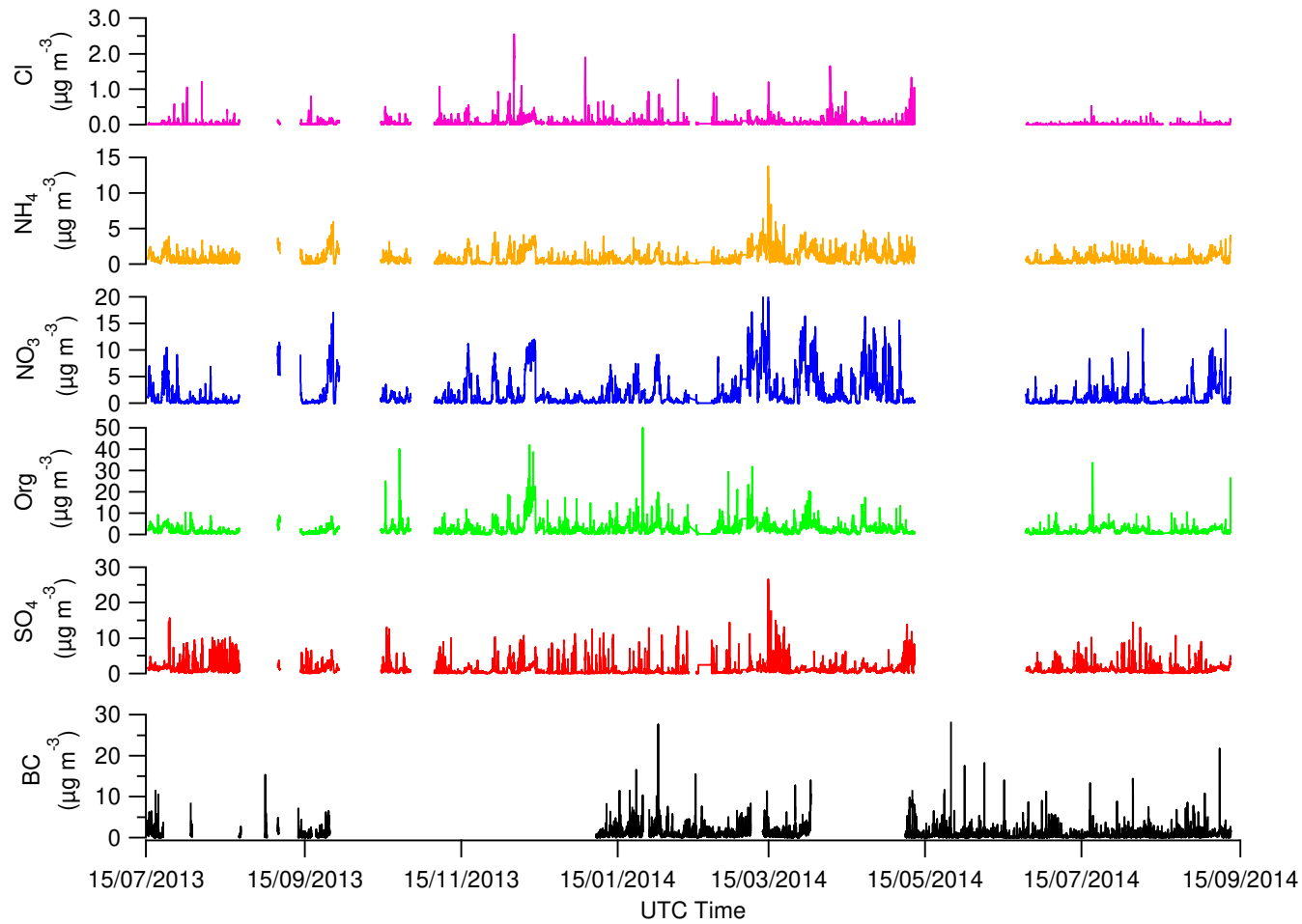


870 (a)



871 (b)

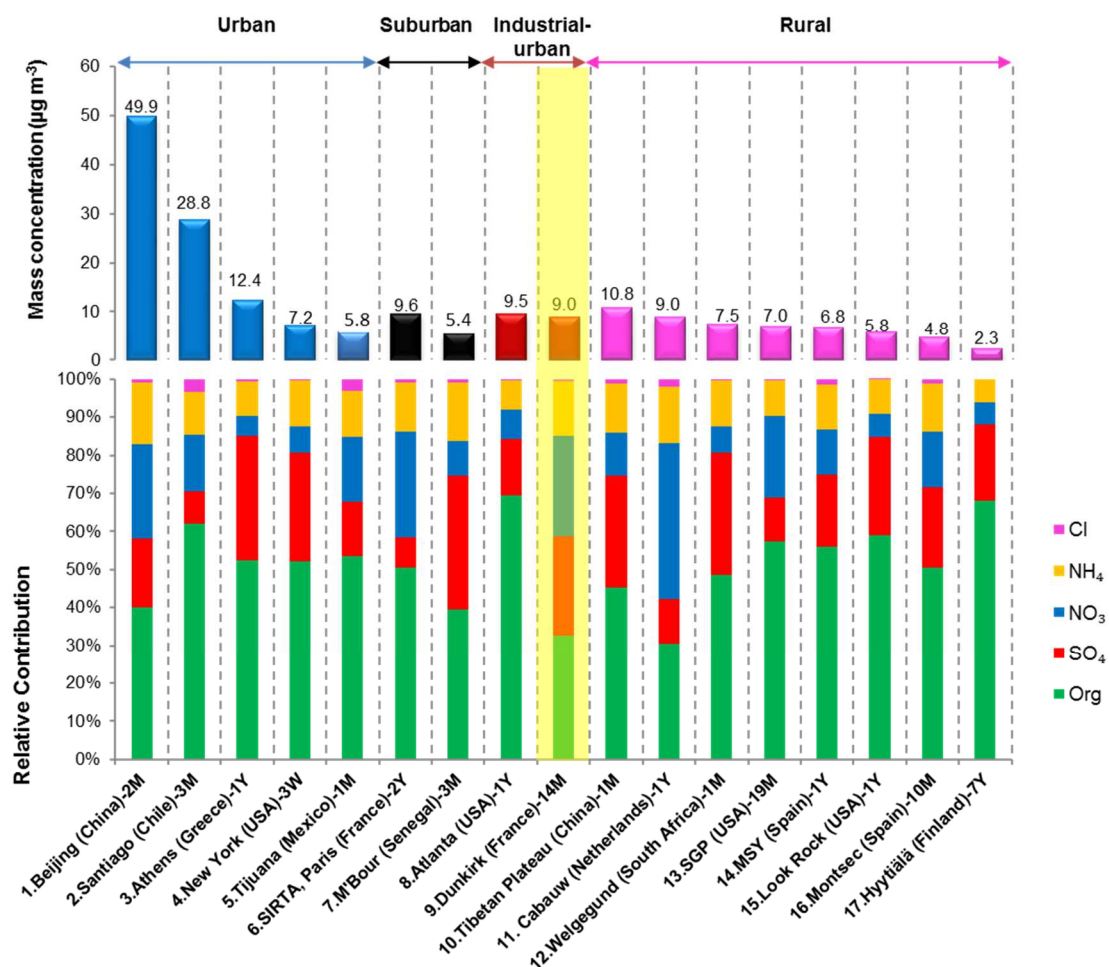
872 Figure 3. (a) Time series of NR-PM₁+BC measured by ACSM+aethalometer vs. Total PM₁
 873 measured by TEOM-FDMS; (b) Scatter plot of PM₁ concentrations (NR-PM₁+BC vs. Total
 874 PM₁): averaged to ACSM time (grey) and 24-h averaged concentration (red). Linear fit
 875 performed on 24-h averaged values.



876

877 Figure 4. Time series of the chemical composition of NR-PM₁ measured by ACSM (Cl, SO₄, NH₄, NO₃, and Org), and Black carbon measured

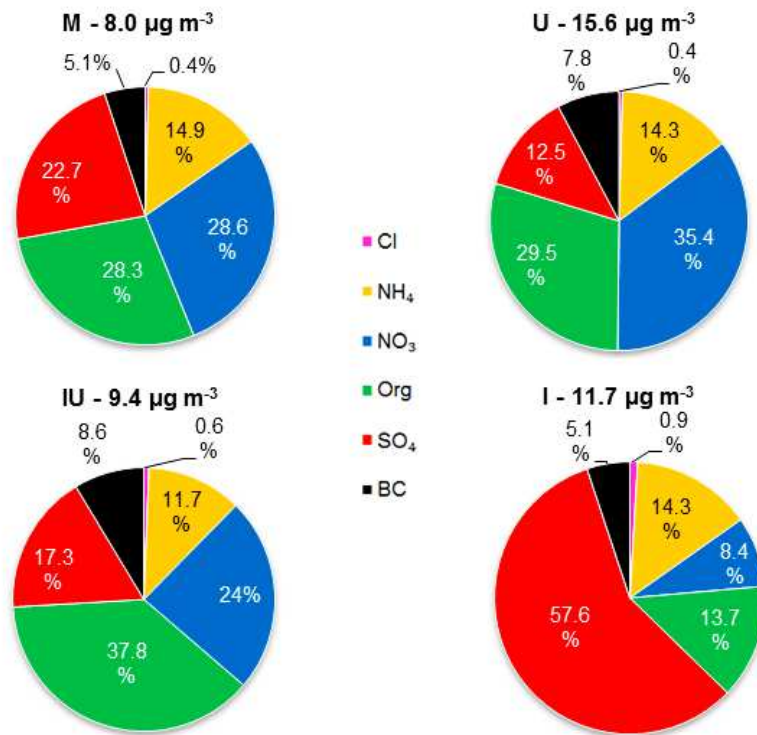
878 by aethalometer.



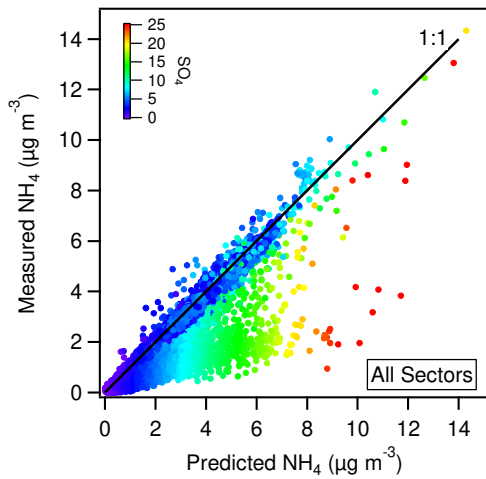
879

880 Figure 5. Comparison of averaged concentrations and chemical compositions of NR-PM₁ for
 881 this study and other ACSM field campaigns. Details on the location and duration of each
 882 campaign are given on the horizontal axis (M: months; W: weeks; Y: year). SGP: Southern
 883 Great Plains, MSY: Montseny.

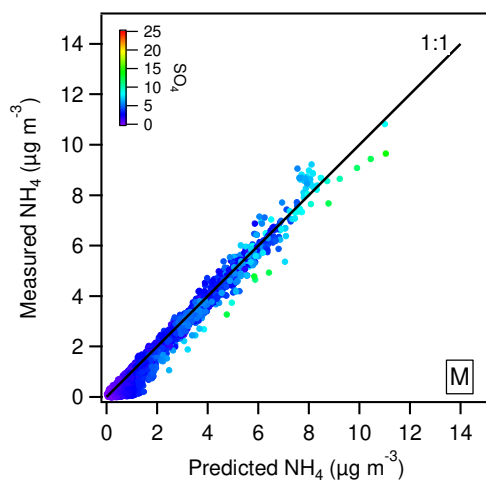
884 1. Beijing (China) (Sun et al. 2012); 2. Santiago (Chile) (Carbone et al. 2013); 3. Athens (Greece) (Stavroulas et
 885 al. 2019); 4. New York (USA) (Ng et al. 2011); 5. Tijuana (Mexico) (Takahama et al. 2013); 6. SIRTA, Paris
 886 (France) (Petit et al. 2015); 7. M'Bour (Senegal) (Rivellini et al. 2017); 8. & 15. Atlanta (USA) and Look Rock
 887 (USA) (Budisulistiorini et al. 2015); 9. This study; 10. Tibetan Plateau (China) (Du et al. 2015); 11. Cabauw
 888 (Netherlands) (Schlag et al. 2015); 12. Welgegund (South Africa) (Tiitta et al. 2014); 13. SGP (USA) (Parworth et
 889 al. 2015); 14. SMY (Spain) (Minguillón et al. 2015); 16. Montsec (Spain) (Ripoll et al. 2015). 17. Hyytiälä
 890 (Finland) (Heikkinen et al. 2020)



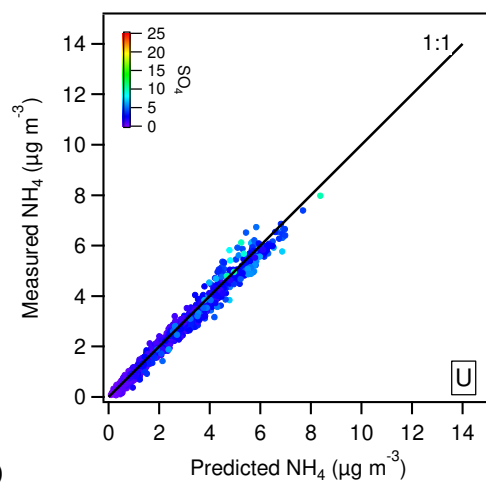
891 Figure 6. Chemical speciation of PM₁ for the four wind sectors (M: marine, U: urban, IU:
 892 industrial-urban, I: industrial).



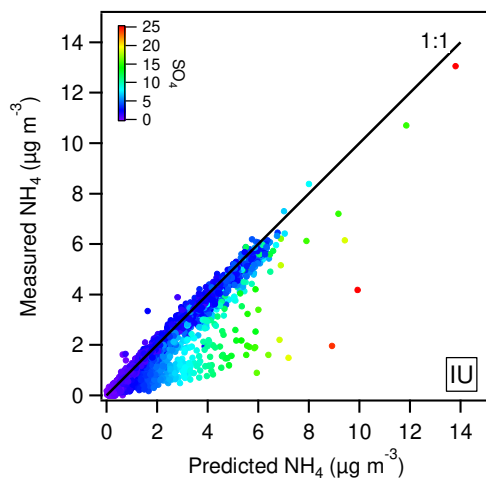
893 (a)



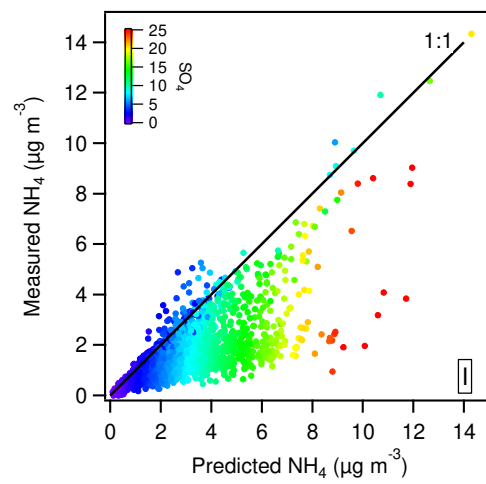
894 (b)



(c)

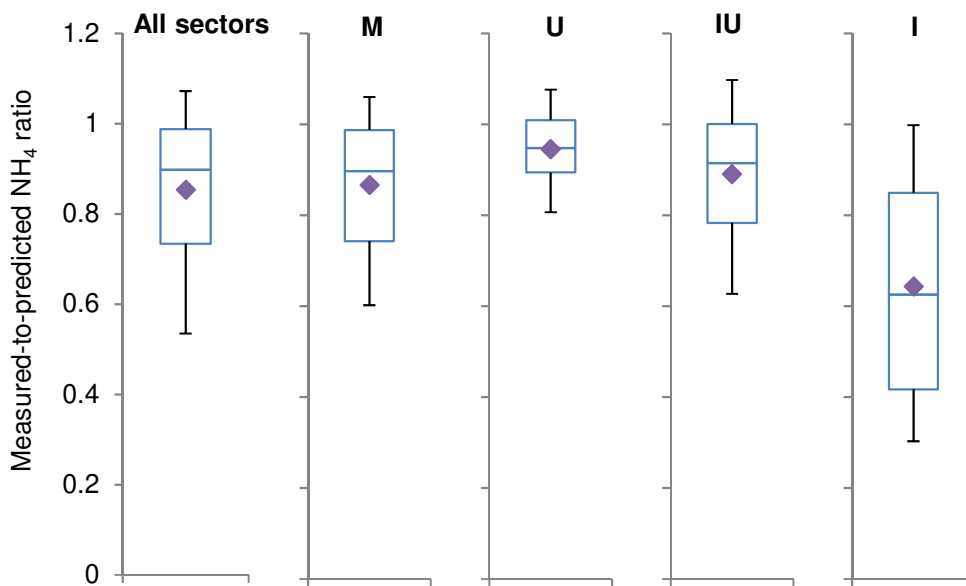


895 (d)

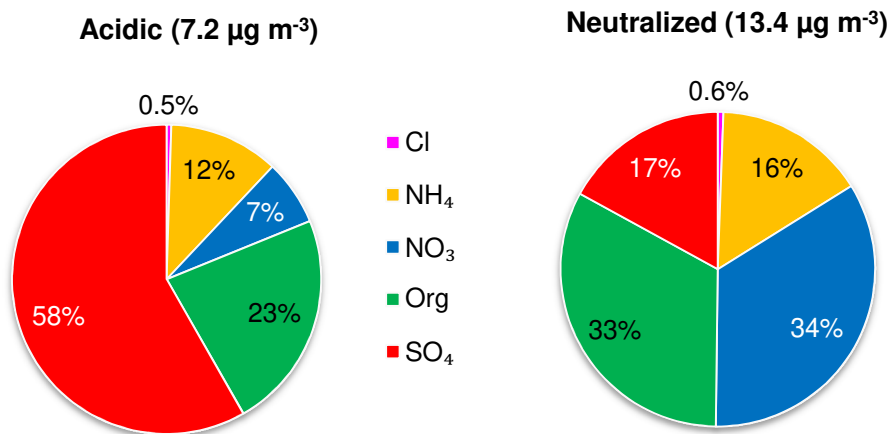


(e)

896 Figure 7. Correlation between measured and predicted NH_4 color coded by the sulfate
 897 concentration ($\mu\text{g m}^{-3}$) (a) for the entire study and (b) – (e) for marine (M), urban (U),
 898 industrial-urban (IU) and industrial (I) wind sectors, respectively. The black line represents
 899 the 1:1 line.

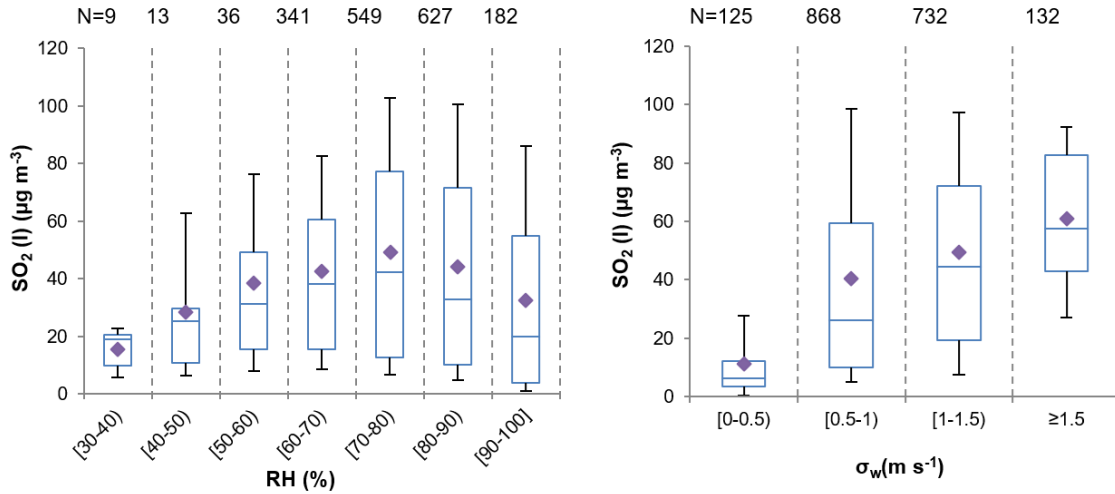


900 (a)

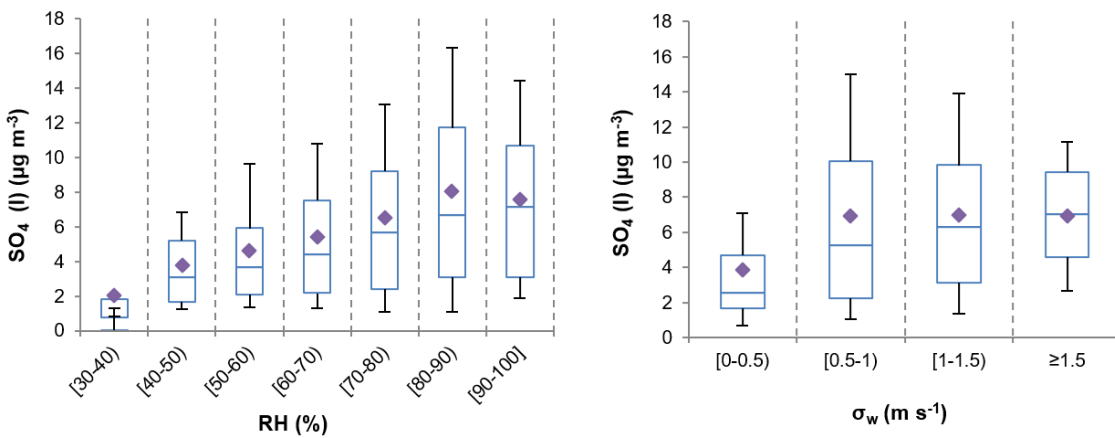


901 (b)

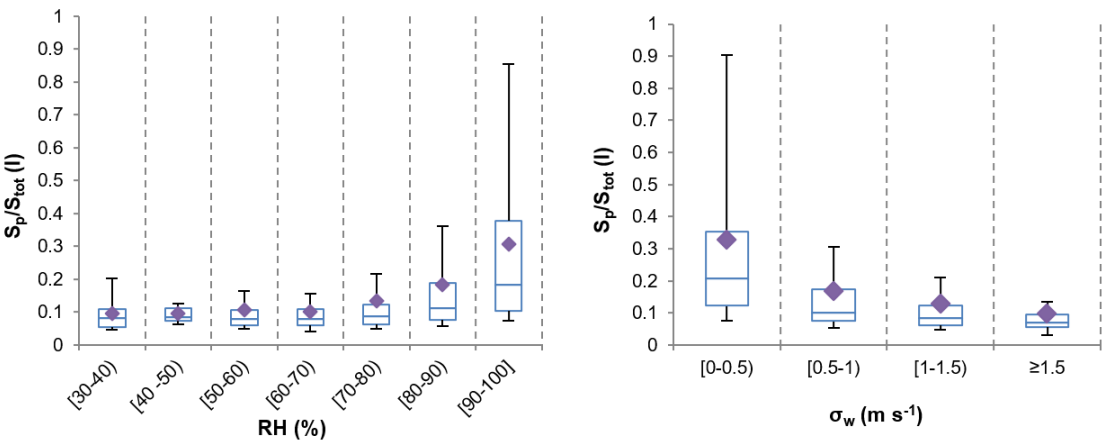
902 Figure 8. (a) Box plots of the measured-to-predicted NH_4 ratio for the entire study and the
 903 four wind sectors. The data correspond to the mean (diamond), median (horizontal line), 25th
 904 and 75th percentiles (lower and upper boxes), and 10th and 90th percentiles (lower and upper
 905 whiskers). (b) Chemical speciation of NR- PM_{10} species for (left) acidic particles (measured-to-
 906 predicted ratio less than 0.75) and (right) neutralized particles (ratio between 0.85 – mean
 907 value – and 1.07 – 90th percentile).



908 (a)



909 (b)



910 (c)

911 Figure 9. Dependences on relative humidity (left) and σ_w (right) of (a) SO_2 , (b) SO_4 and (c)
 912 the particulate-to-total sulfur ratio within the industrial (I) wind sector. The data correspond to
 913 the mean (diamond), median (horizontal line), 25th and 75th percentiles (lower and upper
 914 boxes), and 10th and 90th percentiles (lower and upper whiskers).

